



## EDITORIAL BOARD

E.O. Paton Electric Welding Institute, Kyiv, Ukraine:

**S.I. Kuchuk-Yatsenko** (*Editor-in-Chief*),

**V.M. Lipodaev** (*Deputy Editor-in-Chief*),

**O.M. Berdnikova, Yu.S. Borisov,**

**V.V. Knysh, V.M. Korzhyk, I.V. Krivtsun,**

**Yu.M. Lankin, L.M. Lobanov, S.Yu. Maksimov,**

**M.O. Pashchin, V.D. Poznyakov,**

**I.O. Ryabtsev, K.A. Yushchenko;**

**V.V. Dmitrik, NTUU**

«Kharkiv Polytechnic Institute», Kharkiv, Ukraine;

**E.P. Chvertko, V.V. Kvasnitsky, NTUU**

«Igor Sikorsky Kyiv Polytechnic Institute»,

Kyiv, Ukraine;

**M.M. Student, Karpenko Physico-Mechanical**

Institute, Lviv, Ukraine;

**M. Zinigrad, Ariel University, Israel;**

**Ya. Pilarczyk, Welding Institute, Gliwice, Poland;**

**U. Reisgen, Welding and Joining Institute,**

Aachen, Germany

### Founders

E.O. Paton Electric Welding Institute

International Association «Welding»

### Publisher

International Association «Welding»

### Translators

A.O. Fomin, I.M. Kutianova

*Editor*

N.G. Khomenko

*Electron galley*

D.I. Sereda, T.Yu. Snegiryova

### Address

E.O. Paton Electric Welding Institute,

International Association «Welding»

11 Kazymyr Malevych Str. (former Bozhenko),

03150, Kyiv, Ukraine

Tel./Fax: (38044) 200 82 77

E-mail: journal@paton.kiev.ua

www://patonpublishinghouse.com/eng/journals/tpwj

State Registration Certificate

KV 4790 of 09.01.2001

ISSN 0957-798X

DOI: <http://dx.doi.org/10.37434/tpwj>

### Subscriptions

12 issues per year, back issues available.

\$384, subscriptions for the printed (hard copy) version,

air postage and packaging included.

\$312, subscriptions for the electronic version

(sending issues of Journal in pdf format

or providing access to IP addresses).

Institutions with current subscriptions on printed version

can purchase online access to the electronic versions

of any back issues that they have not subscribed to.

Issues of the Journal (more than two years old)

are available at a substantially reduced price.

All rights reserved.

This publication and each of the articles contained

herein are protected by copyright.

Permission to reproduce material contained in this

journal must be obtained in writing from the Publisher.

## CONTENTS

### SCIENTIFIC AND TECHNICAL

- Poznyakov V.D., Gaivoronskiy O.A., Klapatyuk A.V., Denysenko A.M. and Shmygelskiy S.V.* Influence of composition of deposited metal and thermodeformation cycle of surfacing on stability of joints of wheel steels with dispersion nitride and solid solution strengthening to cold crack formation ..... 2
- Holovko V.V.* The nature of nonmetallic inclusion distribution in the weld metal structural components at arc welding methods ..... 8
- Kovalchuk M.O., M.V. Iurzhenko, Demchenko V.L., Korab M.G. and Kolisnyk R.V.* Quality and operational characteristics of welded joints of pipes of different-type polyethylenes ..... 12
- Rogante M.* Inside welds: Advanced characterization of residual stresses by neutron diffraction ..... 18

### INDUSTRIAL

- Yushchenko K.A., Yarovitsyn O.V., Nakonechnyi O.O., Volosatov I.R., Fomakin O.O. and Khrushchov G.D.* Development of the technology of reconditioning the sealing element of nozzle blade sector from difficult-to-weld high-temperature nickel alloy of ZhS6 type by microplasma powder surfacing ..... 25
- Galinich V.I., Taganovskiy V.M. and Kuzmenko G.V.* Automatic arc surfacing of working paths of lift gates of Kaniv navigation lock ..... 29
- Maksymov S.Yu., Gavrilyuk A.A. and Krazhanovskiy D.M.* Development of the technology of semi-automatic arc welding for the conditions of overhaul and reconstruction of the linear part of the main gas pipelines of Ukraine ..... 32
- Popil Yu.S., Korzh V.M., Chernyak V.Ya. and Zakharov Ye.A.* Diagnostics of hydrogen-oxygen plasma jet for application in thermal spraying ..... 36

# INFLUENCE OF COMPOSITION OF DEPOSITED METAL AND THERMODEFORMATION CYCLE OF SURFACING ON STABILITY OF JOINTS OF WHEEL STEELS WITH DISPERSION NITRIDE AND SOLID SOLUTION STRENGTHENING TO COLD CRACK FORMATION

**V.D. Poznyakov, O.A. Gaivoronskiy, A.V. Klapatyuk, A.M. Denysenko and S.V. Shmygelskiy**

E.O. Paton Electric Welding Institute of the NAS of Ukraine

11 Kazymyr Malevyeh Str., 03150, Kyiv, Ukraine. E-mail: office@paton.kiev.ua

Current trends in the development of railway transport increase the load on the axle and speed of freight trains. The relevant task is to create technologies for the production and restoration of railway wheels, which provide the extension of their service life in different operating conditions. To solve the specified problem, it is necessary to study the influence of different factors on the technological and operational strength of welded joints of wheel steels with dispersion nitride and solid solution strengthening and develop the technology for restoring the rolling profile of all-rolled wheels of freight cars. It was established that the change in resistance of the HAZ metal of wheel steels with dispersion nitride and solid solution strengthening to delayed fracture is significantly influenced by the carbon content in steel and cooling rate during welding. Diffusion hydrogen, contained in the deposited metal, getting into HAZ, significantly reduces its resistance to delayed fracture. In the new wheel steel, the carbon content should not exceed 0.55 %. Under other conditions, it will be impossible to provide the proper level of resistance of joints to the cold crack formation during surfacing of new railway wheels. 11 Ref., 3 Tables, 4 Figures.

*Key words:* arc surfacing, wheel steel with dispersion nitride and solid solution strengthening, heat-affected-zone, structure, cooling rate, diffusion hydrogen, cold cracks

Today in Ukraine to manufacture wheels of freight cars, wheel steel of grade 2 with a carbon content of 0.55–0.65 % is used [1, 2]. Having a relatively low cost, wheels made of such steel have a sufficiently high reliability during operation. The level of loading on the axle of the wheel pair of freight cars during operation on the railway tracks of Ukraine and the CIS countries amounts up to 23.5 t.

Current trends in the development of mainline railway transport in Ukraine are aimed at increasing the load on axle to 27.5 t and the speed of freight trains to 150 km/h, which leads to the use of wheels of improved strength and wear resistance. In this regard, today several directions of creation of new wheel steels are considered. First, it is proposed to increase the carbon content in steel to 0.75 %, as it is done during the manufacture of wheels in the EU, USA and Japan. This is the simplest way, which does not require additional costs and changes in the technological process of manufacturing railway wheels. However, during operation of such wheels on the main tracks of

Ukraine, this can lead to a sharp increase in defects on the rolling surface.

The second direction is based on microalloying of the existing wheel steel with carbide- and nitride-forming elements, due to which it is possible to provide the dispersion of the metal structure. This will promote the improvement of ductile properties of the wheel metal at a higher level of its strength [3–5]. At the same time, to reduce the probability of «shelled treads» formation on the rolling surface of the wheel, the carbon content in the steel should be limited.

All directions of creation of new wheel steels are actively worked out today. However, to increase the strength of railway wheels, the most promising area of development is microalloying of wheel steel with carbide- and nitride-forming elements. At the same time, while creating new railway wheels of higher strength, it is also necessary to predict whether it will be possible to restore them after wear by surfacing in the conditions of domestic production.

**Investigation procedures.** *Investigation of the influence of cooling rate during surfacing on the resistance of HAZ metal to delayed fracture.* The investigations were carried out using the method Implant [6, 7] in a specialized installation developed at the PWI. Cylindrical specimens-inserts made of experimental steel were subjected to tests. They did not have a stress concentrator in the form of a notch. The specimens were cut out along the rolled metal. From the same steel the plates with a size of 300×250 mm were prepared, in the hole of which specimens–inserts were placed on the yield fit, which during the tests were welded-on to the plate.

As the object of investigations experimental wheel steels with dispersion nitride and solid solution strengthening (conditional reduction of KS-DnTR3) were used, having the following composition with different carbon content, wt. %:

No.1 — 0.52 C; 0.70 Si; 0.81 Mn; 0.37 Cr; 0.17 V; 0.0173 N; 0.030 S; 0.025 P.

No.2 — 0.64 C; 0.70 Si; 1.30 Mn; 0.42 Cr; 0.15 V; 0.0174 N; 0.030 S; 0.025 P.

For comparison, wheel steel of grade 2 with a carbon content of 0.54 % and steel 65G (0.65 % C) were used.

Welding of the specimens was performed using a wire of a solid cross-section of grade Sv-08G2S with a diameter of 1.2 mm and a flux-cored wire of grade PP-AN180MN/98 (12GSKhNFT alloying system). During welding using wire Sv-08G2S the conditions were as follows:  $I_w = 180\text{--}200$  A;  $U_a = 28\text{--}30$  V;  $v_w = 13\text{--}15$  m/year, wire PP-AN180MN/98:  $I_w = 250\text{--}280$  A;  $U_a = 28\text{--}30$  V;  $v_w = 15\text{--}18$  m/year. The input energy of surfacing in both cases was approximately at the same level and amounted to 8.6–10.0 kJ/cm.

The cooling rate of HAZ metal was changed due to preheating of the plates, which depending on the technological variant of welding varied from 20 to 250 °C. This approach allowed changing the cooling rate  $w_{6/5}$  of welded joints in the range from 25 to 10 °C/s.

Static loading of the specimens was started after cooling to a temperature of 50 °C. The speed of loading to its constant value was approximately 10 MPa/s. As the index of resistance of HAZ metal of welded joints to delayed fracture, critical stresses ( $\sigma_{cr}$ ) were taken, at which the specimen did not break for 24 h.

*Investigation of effect of diffusion hydrogen on resistance of HAZ metal to delayed fracture.* As in preliminary investigations, the quantitative evaluation of the effect of the diffusion hydrogen content in the deposited metal ( $[H]_{diff}$ ) on the resistance of the HAZ metal to delayed fracture was performed applying the Implant method. As the object of investigations, the experimental wheel steel KS-DnTR3 No.1 with a carbon content of 0.52 % was used. During the tests a

mechanized method of surfacing in a mixture of gases 82 % Ar + 18 % CO<sub>2</sub> was used applying the flux-cored wire PP-AN180MN/98. The specimens were deposited during preheating to a temperature of 100 °C. Under such conditions of surfacing, the cooling rate  $w_{6/5}$  amounted to 12–15 °C/s, and in the HAZ metal a martensitic-bainitic structure was formed, where the volume fraction of martensite was approximately 85 % and the hardness of the quenched metal was in the range of 4440–4640 MPa.

The hydrogen content in the deposited metal was regulated by changing the temperature and time of the flux-cored wire annealing. To determine the number of  $[H]_{diff}$ , the method of «pencil» test was used, which consisted in the following. A specimen of weld metal with the size of approximately 60×14×14 mm was deposited into a copper water-cooled mold. Then, directly after surfacing it was extracted from the mold and additionally cooled in the water flow till the room temperature (cooling time is 10 s) and placed to the eudiometer, where as a locking medium a hydrogen solution of glycerol was used, preheated to the temperature of 40–45 °C. The process of evolution of diffusion hydrogen from the deposited metal specimens lasted for 72 h until its complete cessation. The amount of diffusion hydrogen was calculated by the following formula

$$[H]_{diff} = \frac{ah}{P} \cdot 100 \text{ ml/g},$$

where  $a$  is the coefficient of the eudiometer;  $h$  is the height of the column in the eudiometer, mm;  $P$  is the weight of the specimen of deposited metal, g.

*Investigations of resistance of joints to cold crack formation.* Investigations of the stability of joints of wheel steels with dispersion nitride and solid solution strengthening to cold crack formation were performed during welding of technological specimens «rigid seal welding» [6, 8].

The rigid specimen represents a massive plate with a size of 300×400 mm and a thickness of 45 mm, to which around the whole perimeter the plates of the butt joint with a V-shaped opening (angle is 60°) of the investigated steel with 20 mm thickness, 300 mm length and 100 mm width are welded-on with the leg of 10–12 mm. The total 200 mm width of the joint corresponds to the maximum level of the specimen rigidity — the level of residual tensile stresses in the HAZ metal is approximately 400 MPa [9]. Further, the butt joint is welded with a constructive lack of fusion (gap is 1.5–2.0 mm, blunting is  $h = 4$  mm), which is a stress concentrator for cold crack formation. Welding of specimens during testing of welded joints of experimental wheel steels for resistance to cold crack

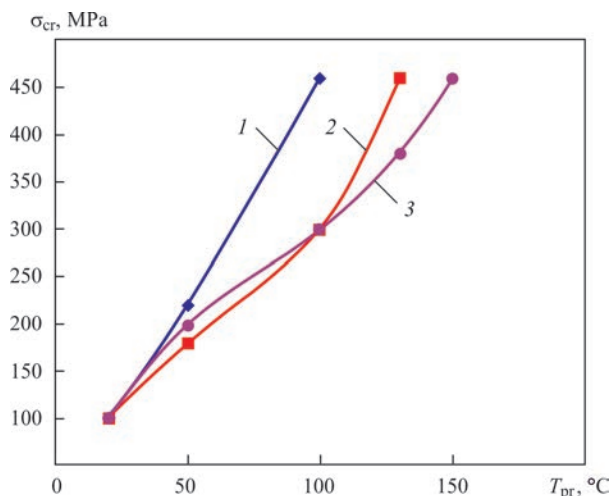


**Figure 1.** Resistance of HAZ metal of wheel steels of grade 2 (1) [11] and KS-DnTR3 No.1 (2, 3) to delayed fracture: 1, 2 — Sv-08G2S; 3 — PP-AN180MN/98

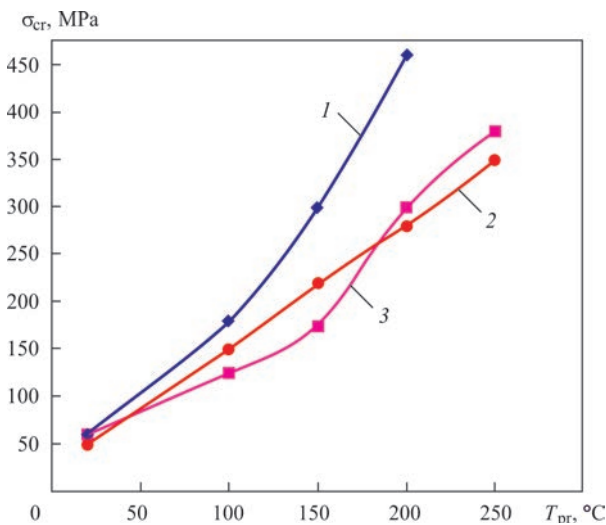


**Figure 2.** Resistance of steel of grade 65G (1) [11] and wheel steel KS-DnTR3 No.2 (2, 3) to delayed fracture of HAZ metal: 1, 2 — Sv-08G2S; 3 — PP-AN180MN/98

formation was performed applying the mechanized method in shielding gases (82 % Ag + 18 % CO<sub>2</sub>) using flux-cored wire PP-AN180MN/98 with a diameter of 2.0 mm on the following conditions: welding current is 250–300 A, arc voltage is 28–30 V, welding speed is 15–18 m/h.

**Table 1.** Parameters of thermal cycle in the HAZ metal during arc surfacing of specimens applying the Implant method

Input energy $Q_{surf}$ , kJ/cm	Preheating $T_{pr}$ , °C	Thermal cycle parameters		
		$w_{6/5}$ , °C/s	$\tau_{8/5}$ , s	$\tau_{8/1}$ , s
8.6–10.0	–	25–30	8	170
	50	20–25	10	230
	70	15–20	11	250
	100	12–15	12	450
	150	8–10	14	760
	200	5–7	18	890
	250	3–4	25	1050

Multilayer welding was performed under the conditions when after each layer of deposited metal the joint was cooled to a temperature of 20–30 °C, after which filling of the groove was continued. To fix the moment of formation and the process of cold crack propagation during cooling of a butt after welding, the method of acoustic emission was used [10]. After welding, the specimens were subjected to 3 days exposure. Further, the reference butt joint was separated from the plate and mechanically cut on templates, from which macro-sections were later made to carry out visual inspection for the presence of cold cracks. The templates were cut out in the places of welded joints, where the most intense acoustic signals were recorded.

**Results of experiments and their analysis.** The generalized results of testing specimens applying the Implant method on determination of the effect of preheating temperature (cooling rate in HAZ) on the resistance of the deposits of the experimental wheel steel with a carbon content of 0.52 and 0.64 % to delayed fracture are presented respectively in Figures 1 and 2.

During surfacing with preheating of metal to 100 °C, the cooling rate in HAZ is reduced to 12–15 °C/s (Table 1). Under such conditions of cooling, the formation of the metal structure in the comparable wheel steels is already significantly different. Thus, in the HAZ metal of wheel steel of grade 2 a bainitic-martensitic structure is formed, in which the share of martensite does not exceed 30 %, and in the experimental wheel steel KS-DnTR3 No.1 the martensitic-bainitic structure is formed, in which the volume fraction of martensite is already predominant and amounts up to 80 %. According to structural differences, the resistance of steels to delayed fracture also changes. During preheating at a temperature of 100 °C, the critical fracture stresses for KS-DnTR3 No.1 are approximately 1.5 times lower. For the wheel steel of grade 2 (0.58 % C) this preheating temperature is already optimal to prevent the development of delayed fracture processes in the HAZ metal during surfacing, and for wheel steel with dispersion nitride and solid solution strengthening (0.52 % C) is still insufficient.

It is possible to increase the critical fracture stresses for the HAZ metal of the experimental wheel steel KS-DnTR3 No.1 to the level of the wheel steel of grade 2 ( $\sigma_{cr} = 460$  MPa) by increasing the heating temperature to 130 °C. Under such conditions, the cooling rate is reduced to 8 °C/s and in the HAZ metal of the experimental steel a strengthening structure is formed, in which the share of martensite does not exceed 50 %. According to the preliminary data, such share of martensite in the structure is critical for a significant probable increase in resistance of the

quenched HAZ metal of high-carbon steels to delayed fracture [11].

It should be noted that during surfacing using the flux-cored wire PP-AN180MN/98 similar results were obtained. In contrast to the variant of welding using the wire Sv-08G2S, it was possible to significantly inhibit the development of delayed fracture processes ( $\sigma_{cr} = 460$  MPa) in the HAZ metal of the wheel steel KS-Dn-TR3 with a carbon content of 0.52 % (experimental steel No.1) at a temperature of preheating of 150 °C.

The indices of critical fracture stresses during the tests of specimens of the experimental wheel steel KS-DnTR3 No.2 with a carbon content of 0.64 % as compared to steel 65G (0.65 % C), differ more significantly (Figure 2) than in the previous case while comparing wheel steels of grade 2 and KS-DnTR3 No.1 (0.52 % C).

The critical cooling rate, at which up to 50 % of martensite is formed in the HAZ metal structure of steel 65G, amounts to 6–7 °C/s, which can be achieved by surfacing with an input energy of 8.6–10.0 kJ/cm using preheating to a temperature of 200 °C. At such a cooling rate in the HAZ metal of the experimental wheel steel KS-DnTR3 No.2, the share of martensite is predominant and amounts to approximately 99 %. Therefore, the critical fracture stresses of the HAZ metal of the experimental wheel steel are more than 1.5 times lower. Even at an increase of preheating temperature to 250 °C, the level of resistance of the HAZ metal of steel KS-DnTR3 No.2 to delayed fracture increases to 350–380 MPa, but still does not reach the level ( $\sigma_{cr} = 460$  MPa), when the development of processes of a delayed fracture is impossible.

The data on the content of diffusion hydrogen in the deposited metal, depending on the conditions of preparation of the flux-cored wire PP-AN180MN/98 before surfacing are given in Table 2.

The generalized results of investigations of influence of the content of diffusion hydrogen in the deposited metal on the indices of the HAZ metal resistance of the experimental wheel steel KS-Dn-TR3 No.1 to the delayed fracture are given in Figure 3.

As is seen from the abovementioned data, at a proper heat treatment of flux-cored wire before surfacing, as it is recommended during its use (annealing at  $T = 230$  °C for 2.5 h), when the content of diffusion hydrogen in the deposited metal is minimal ( $[H]_{diff} = 0.3$  ml/100 g), the critical fracture stresses are the highest and amount to  $\sigma_{cr} = 300$  MPa. Increasing the amount of diffusion hydrogen in the deposited metal to 1.5 ml/100 g leads to a sharp decrease in the resistance of the HAZ metal to delayed fracture. Critical fracture stresses are reduced by almost 2.5 times (to 125 MPa). At a further increase in the diffusion hy-

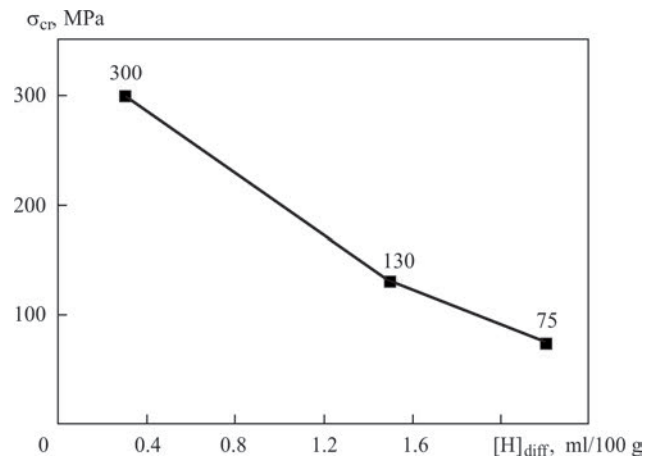


**Figure 3.** Influence of diffusion hydrogen content on resistance of HAZ metal of wheel steel KS-DnTR3 No.1 (0.52 % C) to delayed fracture

drogen in the deposited metal to 2.2 ml/100 g, the processes of delayed fracture proceed even more rapidly and the critical stresses amount to only 75 MPa. As compared to the initial state, when the flux-cored wire was annealed at 230 °C for 2.5 h, the overall decrease in the resistance of the HAZ metal to delayed fracture amounted to 4.5 times.

Therefore, while performing investigations, it was found that in the case of mechanized surfacing of the wheel steel with dispersion nitride and solid solution strengthening, diffusion hydrogen, which is contained in the deposited metal, getting into HAZ, significantly reduces its resistance to delayed fracture. The process of nucleation and propagation of microcracks is accelerated, and the critical fracture stresses at an increase in the content of diffusion hydrogen from 0.3 to 2.2 ml/100 g are reduced to 4.5 times.

The generalized results of tests of technological specimens on resistance of welded joints of experimental wheel steels to cold crack formation are presented in Table 3 and typical examples of cold crack formation are in Figure 4.

While performing tests, it was found that during welding without preheating in welded joints of experimental wheel steels with dispersion nitride and solid solution strengthening, the probability of cold cracks is 100 %. However, depending on the carbon content of wheel steel, there are differences in the nature of cold crack formation and propagation. In welded joints of the wheel steel KS-DnTR3 No.1 (0.52 % C)

**Table 2.** Content of diffusion hydrogen in the deposited metal (wire PP-AN180MN/98)

Conditions for preparation of flux-cored wire before surfacing	$[H]_{diff}$ , ml/100 g
Annealing at $T = 230$ °C for 2.5 h	0.3
Annealing at $T = 200$ °C for 2.5 h	1.5
Without annealing	2.2

**Table 3.** Cold cracks in welded joints of experimental wheel steels KS-DnTR3 No.1 (0.52 % C) and KS-DnTR3 No.2 (0.64 % C) (arc method of welding rigid specimens)

Steel	Welding wire, welding modes	$T_{pr}, ^\circ\text{C}$	Presence and nature of cold crack (CC) formation
KS-DnTR3 No.1, $\delta = 20 \text{ mm}$	PP-AN180MN/98 with a diameter of 2.0 mm, $I_w = 250\text{--}300 \text{ A}$ , $U_a = 28\text{--}30 \text{ V}$ , $v_w = 15\text{--}18 \text{ m/h}$	Without preheating	CC from the concentrator in HAZ and the weld along the fusion line for the entire thickness of the joint
		100	CC were not detected
		150	
KS-DnTR3 No.2, $\delta = 20 \text{ mm}$		Without preheating	CC from the concentrator in HAZ to a depth of 5 mm, then along the weld for the entire thickness and length of the joint
		150	
		200	
		250	

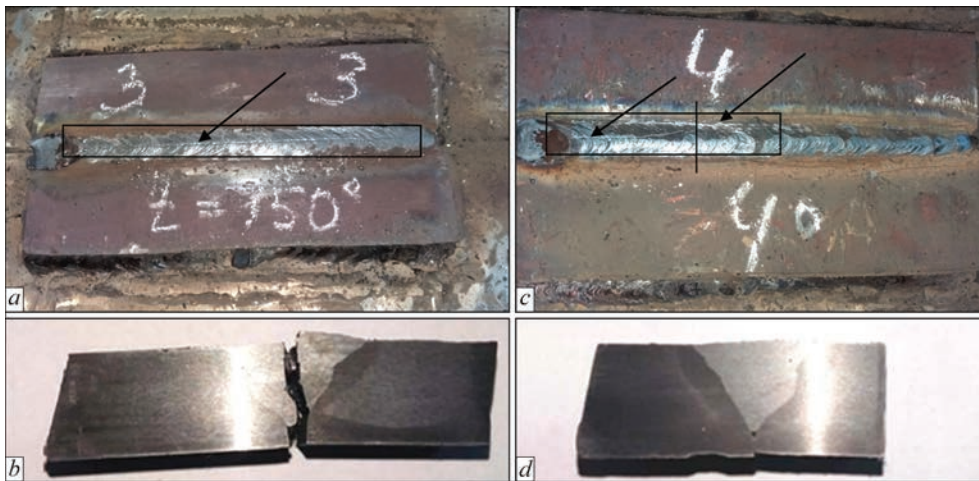


**Figure 4.** Examples of cold crack formation in welded joints of experimental wheel steels with dispersion nitride and solid solution strengthening in welding using flux-cored wire PP-AM180MN/98: *a* — KS-DnTR3 No.2,  $T_{pr} = 150 \text{ }^\circ\text{C}$ , through CC (HAZ, weld); *b* — KS-DnTR3 No.2,  $T_{pr} = 200 \text{ }^\circ\text{C}$ , through CC (HAZ, weld); *c* — KS-DnTR3 No.1, welding without preheating, CC from concentrator in HAZ along the fusion line for the entire thickness of the joint; *d* — KS-DnTR3 No.1,  $T_{pr} = 100 \text{ }^\circ\text{C}$ , CC are absent

a cold crack is formed from the concentrator and propagates in two directions. As is seen from Figure 4, *c* a cold crack propagates along the weld metal (area from the crater of up to 100 mm long), passing further into the HAZ along the fusion line (area of up to 50 mm long) and extends to the joint surface. In both cases, a crack originates in the HAZ metal. At the same time, the total length of a crack amounts to approximately 50 % of the length of the welded joint.

In welded joints of the wheel steel KS-DnTR3 No.2 (0.64 % C) a cold crack is formed from the concentrator, it has the beginning in HAZ, as in the previous case, propagates to the depth to 5 mm, and further — exclusively along the weld to the entire thickness of the joint, also coming to the surface. In this case, the fracture occurs along the entire length of the welded joint.

It is possible to avoid the cold crack formation in welded joints of the wheel steel KS-DnTR3 No.1 (0.52 % C) by applying preheating of the metal to a temperature of 100 °C. During welding of the wheel steel KS-DnTR3 No.2 (0.64 % C), cold cracks are formed even at preheating to a temperature of 250 °C.

Welding of the technological specimen of this steel at a higher preheating temperature was not performed.

**Conclusions**

1. The change in resistance of the HAZ metal of wheel steels with dispersion nitride and solid solution strengthening to delayed fracture is significantly influenced by the carbon content in steel and cooling rate during welding. In surfacing using a wire of a solid cross-section of grade Sv-08G2S or a flux-cored wire of grade PP-AN180MN/98 (12GSKh1NFT) at an input energy of 8.6–10.0 kJ/cm, an increased resistance to delayed fracture is provided under the conditions when the carbon content in the wheel steel does not exceed 0.55 %. Here, the preheating temperature should be up to 150 °C. At a higher content of carbon, the preheating temperature should be increased to not lower than 250 °C.

2. In mechanized surfacing of the wheel steel with dispersion nitride and solid solution strengthening, diffusion hydrogen, which is contained in the deposited metal, getting into HAZ, significantly reduces its resistance to delayed fracture. Therefore, the content

of diffusion hydrogen in the deposited metal should be limited to not more than 0.3 ml/100 g, which is possible at a preliminary annealing of a flux-cored wire PP-AN180MN/98 (12GSKh1NFT) before its use at a temperature of 230 °C during 2.5 h. At a higher content of diffusion hydrogen in the deposited metal, the process of nucleation and propagation of microcracks in the HAZ metal is accelerated, and the critical fracture stresses are reduced by up to 4.5 times.

3. During welding of experimental wheel steels with dispersion nitride and solid solution strengthening, the formation and propagation of cracks in the deposits is significantly affected by the structural state of HAZ metal, which depends on the carbon content in steel and cooling rate. It is possible to avoid cold crack formation under the conditions when the carbon content in steel does not exceed 0.55 % by applying preheating of metal to 100–150 °C.

1. Uzlov, I.G. (2019) Advanced processes of manufacturing and quality of railway wheels. *Stal*, **5**, 69–72 [in Russian].
2. *Railway wheels and treads KLV. Ukraine, Interpipe NTRP* [in Russian] [www.interpipe.biz](http://www.interpipe.biz)

3. Uzlov, I.G., Babachenko, A.I., Dementieva, Zh.A. (2005) Influence of microalloying of steel on fracture toughness of railway wheels. *Metallurgiya i Gornorudnaya Promyshlennost*, **5**, 46–47 [in Russian].
4. Babachenko, A.I., Litvinenko, P.L., Knysh, A.V. et al. (2011) Improvement of chemical composition of steel for railway wheels providing their increased resistance to defect formation on roll surface. In: *Fundamentals and applied problems of ferrous metallurgy. Ukraine, IFM*, **23**. 226–233 [in Russian].
5. Ivanov, B.S., Filipov, G.A., Demin, K.Yu. et al. (2007) Modification of wheel steel by nitrogen. *Stal*, **9**, 22–25 [in Russian].
6. Makarov, E.L. (1981) *Cold cracks in welding of alloyed steels*. Moscow, Mashinostroenie [in Russian].
7. Hrivnak, I. (1984) *Weldability of steels*. Moscow, Mashinostroenie [in Russian].
8. Gaivoronsky, A.A. (2013) Cold crack formation in welding of high-strength carbon steel. *Svarka i Diagnostika*, **5**, 27–32 [in Russian].
9. Poznyakov, V.D. (2008) Improvement of delayed cracking resistance of welded joints of cast hardenable steels. *The Paton Welding J.*, **5**, 7–12.
10. Musiyachenko, V.F., Zhdanov, S.L. (1981) Study of mechanism of cold crack development by acoustic emission method. In: *Cracks in welded joints*. Bratislava, 130–136.
11. Gaivoronsky, A.A. (2014) Resistance to cold crack formation of HAZ metal of welded joint on high-strength carbon steels. *The Paton Welding J.*, **2**, 2–11.

Received 02.11.2020

WORLD TRADE FAIR FOR WELDING ENGINEERING —  
JOINING, CUTTING, SURFACING

LET'S JOIN  
THE WORLD!

13. – 17. September, 2021

REGISTER NOW!

[www.schweissen-schneiden.com](http://www.schweissen-schneiden.com)

DVS GERMAN WELDING SOCIETY

MESSE ESSEN

# THE NATURE OF NONMETALLIC INCLUSION DISTRIBUTION IN THE WELD METAL STRUCTURAL COMPONENTS AT ARC WELDING METHODS

V.V. Holovko

E.O. Paton Electric Welding Institute of the NAS of Ukraine  
11 Kazymyr Malevych Str., 03150, Kyiv, Ukraine. E-mail: [office@paton.kiev.ua](mailto:office@paton.kiev.ua)

With the purpose of expert evaluation of welded joint performance a large number of computer programs have been developed now for prediction of the weld metal structural composition and their mechanical properties. Such programs are usually based on multivariate analysis of the processes occurring in the welding arc, and thermodynamics and kinetics of the processes in the weld pool. It should be noted that at analysis of crystallization and recrystallization reactions in the weld metal, such programs usually do not take into account the nature of nonmetallic inclusion distribution in the structural components. There are many studies, which point to a significant impact of the inclusion, depending on whether they are present on the boundaries or in the body of the grains. The paper shows the need to take into account the probability of nonmetallic inclusions being in the body of structure grains or on their boundaries at construction of the numerical models that will allow improving the correspondence of the predicted data and the experimental results of determination of the mechanical characteristics of weld metal. 5 Ref., 5 Figures.

*Keywords: metals science, low-alloy steels, welds, microstructure, numerical modeling, nonmetallic inclusions*

The impact of nonmetallic inclusions on the structure and properties of welds on iron alloys has been given a lot of attention already for about one and a half centuries. It should be noted that this problem remains relevant over time, and this is related to the change of ideas about the peculiarities of their impact. While the first works provided convincing proof of the negative effect of increased volume fraction of inclusions in welds on formation of metal mechanical properties, later on the researchers found that the size distribution and chemical composition of the inclusions should be taken into account. At the end of the XX century studies were performed, which demonstrated the positive role of certain inclusions in the processes of secondary crystallization of low-alloy steel welds. In studies conducted in recent years, attention was paid to the impact of nanosized inclusions on increasing the level of mechanical properties of welds of high-strength low-alloy steels. Proceeding from the results of scientific research, laboratory testing and industrial practices, one can come to the conclusion that analysis of the impact of nonmetallic inclusions on the structure and properties of welds requires application of a complex approach, which allows not only for the topological indices, but also for the physicochemical characteristics of both the inclusions proper, and the nature of their interaction with the metal solution and the crystalline phase. Here, it was noted more than once that the inclusions impact depends on where ex-

actly they are located: in the center of large grains or on the intergrain or intragrain boundaries. However, while a large scope of research was devoted to the issues of inclusion distribution in welds by size and chemical composition, their impact on formation of the structure and mechanical properties of weld metal, the problem of distribution of inclusions in the microstructural components is given much less attention.

The problem of modeling the processes, which affect formation of weld microstructure, in order to predict the level of its performance, requires conducting multivariate analysis. Modern possibilities of computer processing of large data bases, and numerical analysis of thermodynamics and kinetics of nonequilibrium processes enable solving such tasks. Over the past decade, there were publications, in which the authors show the ability of such an approach to solve the complex problem with optimization of the technology of welded metal structure fabrication, for instance [1–5]. The role of nonmetallic inclusions is taken into account in these works, in terms of their distribution by size and chemical composition. However, the nature of inclusion distribution in the structural components proper is ignored. In our opinion, modeling of the impact of nonmetallic inclusions without allowing for the nature of their distribution in the structural components will not enable sufficiently reliable prediction of the mechanical properties of weld metal.

The work gives an idea about the processes, which determine the nature of distribution of nonmetallic inclusions in the microstructure of metal of low-alloy steel welds.

**Inclusion formation.** Most of the welding processes are accompanied by melting of the base and filler metal simultaneously with slag-forming material in the form of electrode coating, flux-cored wire core, or welding flux. High energy concentration between the melting electrode and weld pool promotes formation of a plasma discharge of up to 20000 K temperature, in which the welding wire and the flux melt, evaporate and decompose into constituent elements. These elements are transferred from the electrode into the weld pool by three main methods (Figure 1):

- as ions in the plasma column;
- as fine drops on the plasma periphery;
- as large drops, which separate from the electrode tip and are transported through the plasma during a brief time period.

In addition, loss of certain elements occurs through evaporation in the welding arc atmosphere.

Welding process parameters have a strong impact on arcing stability, effectiveness and mode of element transfer into the weld pool. Therefore, despite, for instance, the fact that the flux almost entirely consists of oxides and fluorides, they are not transferred through the arc in the form of the initial compounds at all, but rather as constituent elements. Only rather coarse particles of the electrode coating, which are capable of remaining unchanged while passing through the welding arc, can penetrate into the weld pool and significantly impair the mechanical properties of weld metal. The weld pool cast metal ( $T > 2600\text{ }^{\circ}\text{C}$ ) contains alloying elements (Ti, Al, Si, Mn, etc.), which passed from the welding material and base metal, and a large amount of oxygen, as its solubility in liquid alloys of iron with carbon is high (0.22–0.29 % in iron melting point) and rises (up to 0.33 %) at 1700 °C.

Oxygen comes from the ambient atmosphere or from the shielding gas, which often has  $\text{CO}_2$  in its composition. This process should be controlled, as oxygen content in metal drops at the electrode tip can be up to 5000 ppm, and this requires a large amount of deoxidizers for oxygen removal from the weld pool at its cooling. In addition, presence of oxides in the flux, which readily decompose ( $\text{SiO}_2$  type), leads to increase of oxygen content in the weld metal, which enters it from the slag. Increase of the content of higher basicity compounds ( $\text{CaO}$ ,  $\text{MgO}$  and  $\text{CaF}_2$ ) in the flux promotes reduction of the amount of oxygen in the weld, although oxygen potential and basicity are not necessarily connected. In welding using highly basic fluxes, oxygen content can be lowered to the level below 200 ppm, but this necessitates application of such strong deoxidizers as aluminium. Depending on their tendency to oxidize, the oxides can be arranged in a certain sequence, and oxygen potential can be deter-

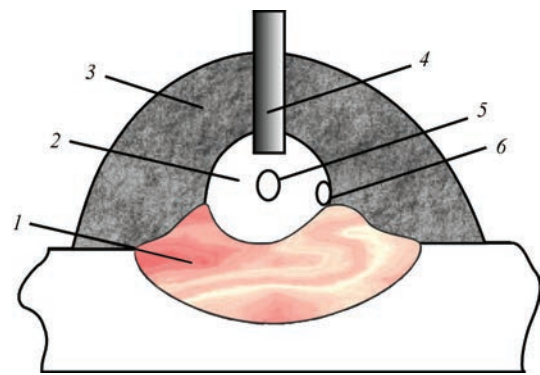


**Figure 1.** Main modes of chemical element transfer in the welding arc: 1 — weld pool; 2 — plasma; 3 — flux; 4 — electrode; 5 — large drops in arc column; 6 — drops on the periphery

mined based on partial pressure of oxygen, which is found from the decomposition energy of pure oxides. The oxides were arranged in the direction of lowering of their tendency to decompose, in the following order:  $\text{SiO}_2 > \text{TiO}_2 > \text{Al}_2\text{O}_3 > \text{ZrO}_2$ .

In arc welding methods with slag phase participation, oxygen transfer is determined by the conditions of  $\text{FeO}$  formation in the slag, as a result of flux oxide decomposition. The amount of  $\text{FeO}$  which enters the weld pool, increases with reduction of free energy of flux oxide formation, so that  $\text{MnO}$ ,  $\text{SiO}_2$  and  $\text{Cr}_2\text{O}_3$  essentially affect weld metal oxidation. In most cases, however, up to 90 %  $\text{FeO}$  is removed from weld pool metal into the slag.

Oxygen solubility in iron drops abruptly with temperature lowering (at 1345 °C oxygen solubility in  $\gamma$ -iron is equal to 0.003–0.007 wt.%), here the driving force of oxide formation becomes greater. This results in appearance ahead of crystallization front, of predominantly oxide particles with a higher temperature of formation, i.e. it can be assumed that refractory oxides, based on Al, Si and Ti form in the metal melt in a homogeneous manner. Such conditions of inclusion formation can be predicted, proceeding from Ellingham diagram (Figure 2).

**Processes, controlling inclusion distribution in weld metal structure.** The strongest oxides are located in the lower part of the diagram and form at a lower activity of oxygen, assuming that its activity is constant over the entire metal volume. Silicates form at much lower temperatures, than do oxides. On the whole, it is real to assume that they form during the process of metal solidification in interdendritic spaces which are enriched with impurity and alloying elements. This process can be promoted by presence of primary high-temperature oxides. Such a conclusion is confirmed by the nature of location of inclusions in interdendritic spaces (Figure 3).

The resultant complex of inclusions is determined by the time of segregation action and of inclusions growth, so that in the general case the oxides should

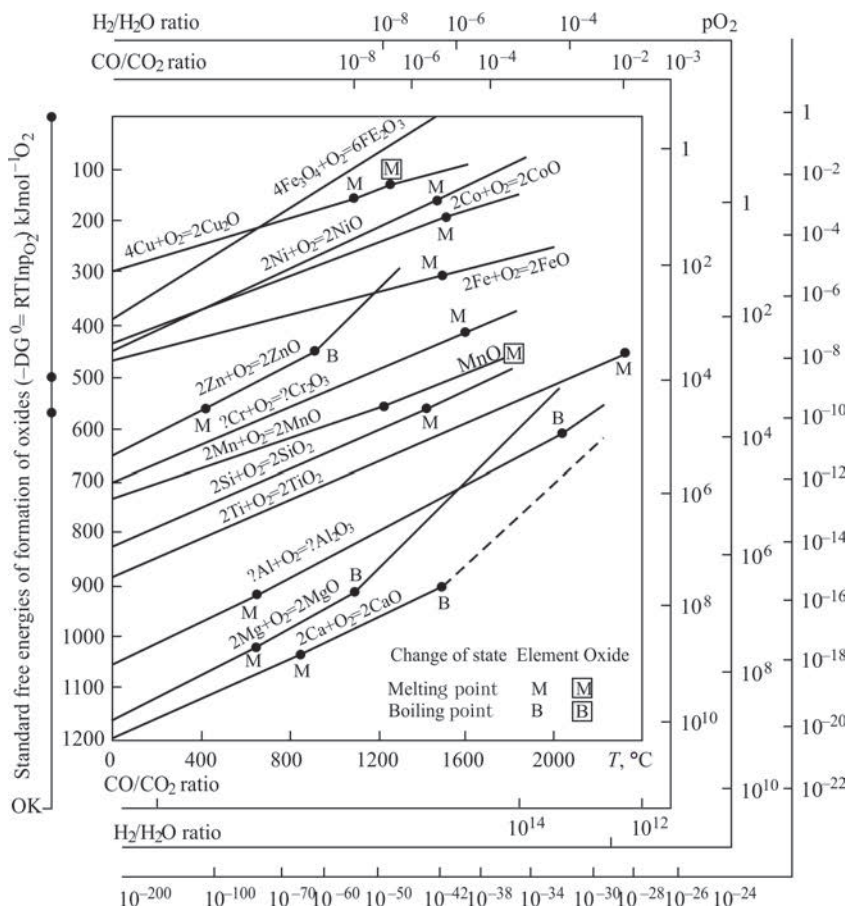


**Figure 2.** Ellingham diagram of the change in free energy of oxide formation

be larger ( $> 1 \mu\text{m}$ ) than the silicates, as they are able to grow for a longer time. However, as the oxides form in a melt with high flow velocities and turbulence, a certain part of them is removed into the slag, others can be carried to the high-temperature zone of the melt, where their dissociation takes place. The process of separation of nonmetallic inclusions from the weld pool does not reach its completion, as certain particles are entrained by the solidifying metal front, thus forming an inclusion population in it.

Stokes law, that is flotation and separation as a result of the impact of the lifting force, does not apply to inclusions in the weld pool metal, because of

insufficient time of the action of this force, and also because the metal flows have a much stronger effect. Two regions can be singled out in the weld pool by the intensity of these flows (Figure 4). The «hot» region with very turbulent metal flow, from which the particles are rapidly removed, and the «cold» one, located closer to the pool edges, in which the velocity of flow movement is much lower that leads to entrainment of a larger quantity of particles by the moving crystallization front. This explains why oxygen content in the deposited metal is usually higher than can be anticipated, proceeding from the conditions of thermodynamic equilibrium, approximated to the region of temperatures below the solidification temperature. In

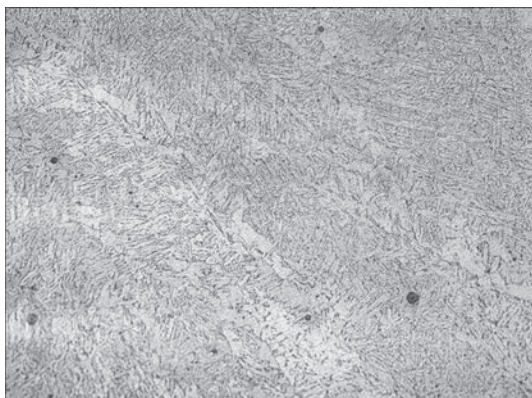


**Figure 3.** Precipitates of coarse nonmetallic inclusions in the grain body ( $\times 200$ )

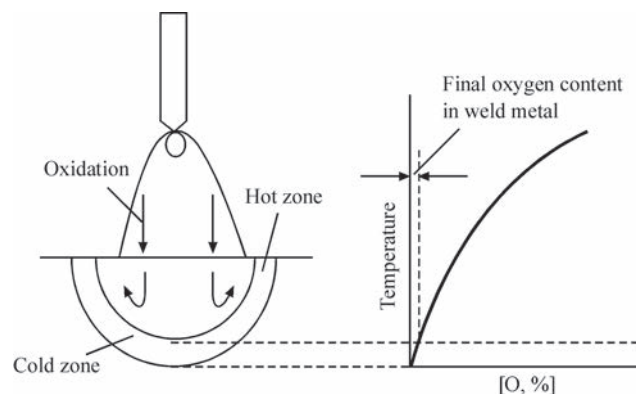


**Figure 4.** «Hot» and «cold» zones of the weld pool

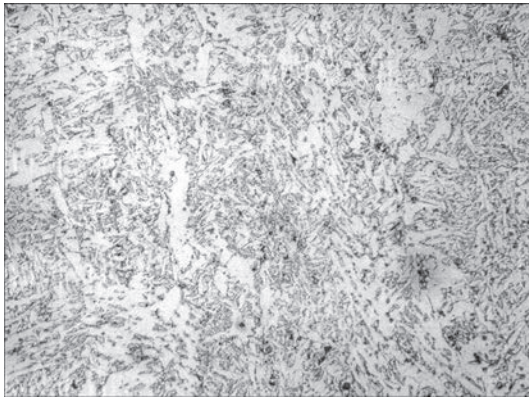


**Figure 5.** Precipitation of silicate inclusions in the form of chains on grain boundaries ( $\times 500$ )

addition, Ellingham diagram applies only to spherical oxides, and gives the standard energy of their formation, referred to one mole of oxygen at this temperature, although high-temperature inclusions can have such carbides and nitrides in their composition with high melting temperature as, for instance TiN.

Interaction of the crystallization front with the inclusions, causes segregation of solid products of deoxidation, associated with segregation of alloying elements. Crystallization front advance can have such an impact on the inclusion, which makes it move forward, ahead of the crystallization front. Other mechanisms of impact can be also manifested, of the type of Marangoni effect, which is the result of the change in interphase tension. The effect of the last type depends essentially on melt composition, as segregation occurring on the crystallization front during the solid-phase growth, is caused by gradients of concentration and interphase tension, which lead to convection, directed towards the solidification boundary. Moreover, surface tension can cause nonuniform distribution of oxide particles. Coarse inclusions are characterized by low mobility, and that is why they are entrapped by the solidifying solution, while finer inclusions accumulate on the interphase front and are distributed along the grain boundaries.

The impact of any forces arising as a result of processes taking place in the melt flows, is proportional to the area of its contact with the inclusion, ( $r^2$  for spherical inclusions), while the particle inertia is proportional to the volume ( $r^3$  for spherical particle). Therefore, the segregation tendency should decrease with increase of the volume/surface ratio at increase of the spherical particle radius. Such dependence can be violated by the effect of particle floating, however, such an effect has not been detected up to now. Silicates, which form later, have a tendency to create a chain of inclusions along the interdendritic boundaries (Figure 5).

Experimental verification of such a nature of segregation is difficult, as the metal structure undergoes transformations during weld cooling, which violate the primary crystallization structure. Application of special etching methods that allow detecting the primary structure boundaries, allows establishing a correspondence between them and inclusion distribution. During weld metal cooling, further growth of inclusions, often in the form of sulphides, takes place, they often precipitating on the already existing inclusions. Many researchers noted the presence of  $\text{Cu}_x\text{S}$  film, which covers the oxide particles in the metal of welds of low-alloy steels. Increase of sulphur content in the weld metal leads to replacement of compounds rich in titanium oxide, by a film of (Cu, Mn) S type in the surface layer of the inclusions.

### Conclusions

Reliable prediction of the structural composition of the metal of welds and their mechanical properties based on multivariate analysis is impossible without application of numerical modeling. With this purpose, researchers developed computer programs, which allow taking into account both the chemical composition of the base metal and welding consumables, and the parameters of welding technology. Application of such programs demonstrated the possibility of greatly increasing the effectiveness of such research developments in the field of fabrication of welded metal structures, on the one hand, and it also showed the presence of a noticeable discrepancy between the calculated data and experimental results in certain situations, which can be related to insufficiently full description of the features of formation of weld metal structure. The work gives an idea on the processes which determine the nature of nonmetallic inclusion distribution in metal microstructure of low-alloy steel welds.

1. Sarma, D.S., Karasev, A.V., Jönsson, P.G. (2009) On the role of non-metallic inclusions in the nucleation of acicular ferrite in steels. *ISIJ Int.*, 49(7), 1063–1074.
2. Cortés, V.H.V., Guerrero, G.A., Granados, I.M. et al. (2019) Effect of retained austenite and non-metallic inclusions on the mechanical properties of resistance spot welding nuggets of low-alloy trip steels. *Metals*, 9(9), 1064; DOI:10.3390/met9101064.
3. Ignatova, A., Ignatov, M. (2015) The measurement of hardness and elastic modulus of non-metallic inclusions in steely welding joints. *TEM J.*, 4(3), 314–318.
4. Pimenov, A.V. (2015) On influence of nonmetallic inclusions on toughness of low-alloy weld metal at low temperatures. *Voprosy Materialovedeniya*, 81(1), 108–110 [in Russian].
5. Kartashov, M.F., Ignatova, A.M., Fedoseeva, E.M., Ignatov, M.N. (2014) Characteristic of nonmetallic inclusions in welded joints of gas-and-oil pipelines. *Neftegazovoe Delo: Electron. J.*, 2, 80–94 [in Russian].

Received 19.10.2020

# QUALITY AND OPERATIONAL CHARACTERISTICS OF WELDED JOINTS OF PIPES OF DIFFERENT-TYPE POLYETHYLENES

**M.O. Kovalchuk, M.V. Iurzhenko, V.L. Demchenko, M.G. Korab and R.V. Kolisnyk**

E.O. Paton Electric Welding Institute of the NAS of Ukraine

11 Kazymyr Malevych Str., 03150, Kyiv, Ukraine. E-mail: kovalchukMAwork@gmail.com

Polyethylene raw materials used for production of polyethylene pipes are constantly being improved. At the beginning of the construction of plastic pipelines, the so-called low pressure polyethylene, currently known as PE-63 grade was used. Subsequently, new, more advanced types of raw materials, which represent a copolymer of polyethylene with hexane, were developed. Today, almost all pressure pipes are made of PE-80 and PE-100 grades of polyethylenes. However, during the repair and reconstruction of plastic pipelines, there is an urgent problem of joining pipes of PE-63, which have been operated for a long time, with new pipes made of polyethylenes of grades PE-80 and PE-100. In the paper, complex investigations of thermophysical properties of technical polyethylenes were carried out and significant differences were revealed, which should be taken into account during the repair of polymer pipelines. Experimental welding of pipe specimens from both single- as well as different-type polyethylenes was carried out. Morphological and mechanical studies of welded joints of polyethylene pipes of grades PE-63, PE-80, and PE-100 were performed. According to the results of investigations, the influence of their thermophysical properties and parameters of the welding process on the morphological structure and quality of welded joints of different-type polyethylenes was determined. Mathematical modeling of temperature fields during butt welding was carried out. A two-zone heating tool for butt welding of pipes with an outer diameter of up to 110 mm of different-type polyethylenes of pipe grades PE-63 and PE-80, PE-100 using a heated tool was designed and created. In order to test an experimental specimen of a two-zone heating tool, a series of experiments were carried out, which showed an improvement in the strength characteristics of the produced welded joints. 8 Ref., 4 Tables, 10 Figures.

*Key words:* polyethylene raw material of different types, polyethylene pipes, welded joints

The problem of repairing polyethylene pipes is important in terms of their safety and reliability of operation. As is known, the old pipelines were built using polyethylene of grade PE-63, which is already technologically outdated and no longer produced, and a complete replacement of the pipeline instead of its separate section is not advisable. Therefore, to provide the repair of such pipelines, it becomes necessary to study the possibility of welding polyethylenes of different grades. In the work the results of complex thermophysical and structural investigations of polyethylenes PE-60, PE-80 and PE-100 are given. The main differences of materials were established affecting the possibility of producing a quality welded joint. Technological approaches to welding of different-type polyethylenes were developed.

At the beginning of the construction of plastic pipelines, the pipes of polyethylene of grade PE-63 were used, but with the development of the polymer industry in the 2000s, it was replaced by more technological polyethylenes of grades PE-80 and PE-100. This has led to a global problem of repair and recon-

struction of old polyethylene pipes because of the need to weld materials with different thermophysical properties and the lack of available information and investigations of the quality characteristics of joints of different-type polymers, even at a short-term use. Joining parts and pipes of different grades of polyethylene have different physical and mechanical properties, and therefore require special technological parameters of their welding process. The available information on the possibilities of welding pipes and parts of polyethylene composites of different types, reliability and service life of their welded joints is significantly contradictory and limited. Some standard documents allow welding different-type polyethylenes between each other, if they have close values of melt viscosity, which is estimated according to the value of melt flow index. However, the problem of optimizing the process of welding heterogeneous polyethylene pipes is not easy and requires additional investigations and appropriate adaptation of welding equipment [1]. While choosing the parameters of the process of welding polyethylene pipes, it is necessary

M.O. Kovalchuk — <https://orcid.org/0000-0003-2161-643X>, M.V. Iurzhenko — <https://orcid.org/0000-0002-5535-731X>,  
V.L. Demchenko — <https://orcid.org/0000-0001-9146-8984>, M.G. Korab — <https://orcid.org/0000-0001-8030-1468>,  
R.V. Kolisnyk — <https://orcid.org/0000-0003-2161-643X>

© M.O. Kovalchuk, M.V. Iurzhenko, V.L. Demchenko, M.G. Korab and R.V. Kolisnyk, 2020

**Table 1.** Characteristic temperatures of thermal oxidative destruction of specimens of technical polyethylenes PE-63, PE-80 and PE-100

Specimen	$T_d$ , °C	$T_{d\max}$ , °C
PE-63	252	418
PE-80	264	420
PE-100	274	450

to take into account the peculiarities of the thermo-physical properties of the base material, as well as the presence and amount of impurities. In particular, the material of pipes that have already been in operation may have impurities that have appeared as a result of adsorption from the environment [2].

**Materials and procedures of investigations.** To perform welding works, as the model objects, polymer pipes with a nominal outer diameter of 63 mm and a wall thickness of 5.8 mm were used, made of three grades of technical HDPE with a different minimum long-term strength MRS, namely PE-63 (density is 0.940 g/cm<sup>3</sup>, MRS6.3 according to GOST 16338 [3], GOST R 50838 «Polyethylene pipes for the supply of gaseous fuels» [4]), PE-80 (density is 0.941 g/cm<sup>3</sup>, MRS8 MPa) and PE-100 (density is 0.954 g/cm<sup>3</sup>, MRS10 MPa) [5, 6].

At the first stage, the thermophysical properties of the polymer material of polyethylene pipes of all three grades were investigated applying differential scanning calorimetry (DSC) in the calorimeter TA Instruments DSC Q2000 and applying thermomechanical analysis (TMA) in the device TA Instruments TMA Q400 EM.

At the second stage, experimental welding of polymer pipes, both single-type as well as those of different grades, was performed using «butt» method with a heated tool according to the conventional flowchart (Figure 1). The parameters of the welding mode were set according to the requirements of the standard [7] – temperature of the heated tool is 210 °C, heating time is 60 s, technological pause is 3 s, upsetting pressure is 0.2 MPa, cooling time under pressure is 6 min.

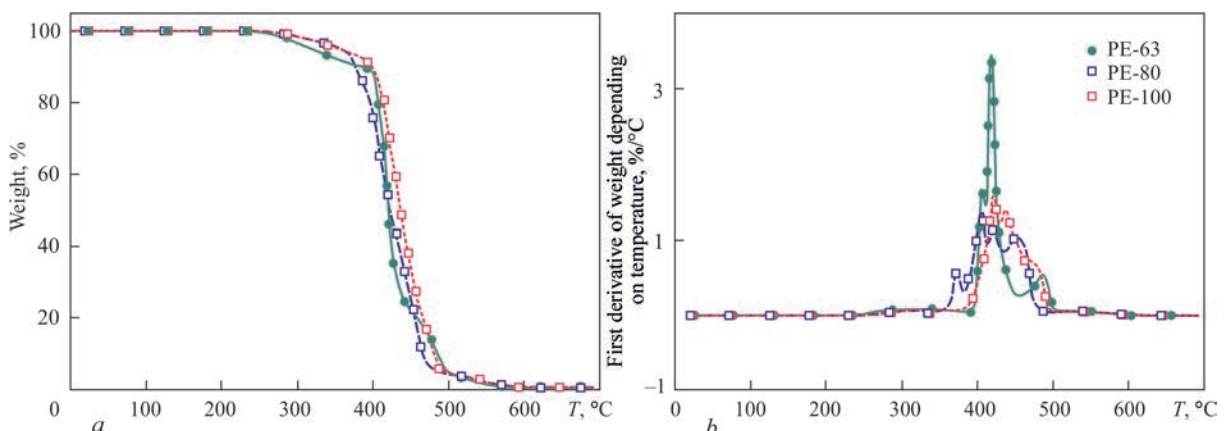


**Figure 2.** TGA of curves of specimens of technical polyethylenes PE-63, PE-80 and PE-100

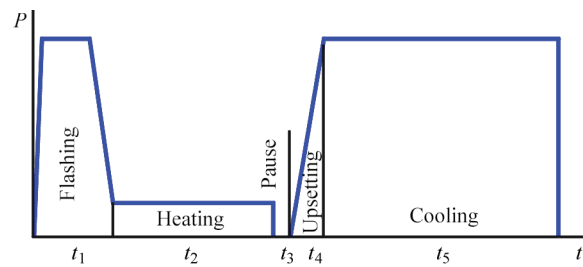


**Figure 1.** Flowchart of conventional process of butt welding using heated tool

At the third stage, the produced welded joints of single- and different-type polymer pipes in different combinations were laid in an environment that simulates the operating conditions — into the ground to a depth of 10 cm, and on the surface, where they were under the influence of climatic factors during 1 and 2 years.

At the fourth stage, comprehensive investigations were carried out to study the long-term effect of the environment on the experimental specimens. The structural features of the specimens were investigated by means of wide-angle X-ray scattering (WAXS in the X-ray diffractometer DRON-4-07) and optical microscopy in the Versamet-2 microscope. The service characteristics of polymer pipe welds were evaluated applying the methods of visual inspection in accordance with DSTU EN13100-1:2017 and mechanical tensile tests in the rupture machine FP-10 in accordance with DSTU EN12814-2:2018 and DBN V.2.5-41.

Thermal processes during welding of pipes of different-type polyethylenes were theoretically investigated applying mathematical modeling using the finite element method.

**Results of thermophysical studies.** Thermogravimetric analysis (TGA) of the specimens of technical polyethylenes showed that as to the character of TGA curves (Figure 2, a), polyethylenes of all three types are similar, however, the temperature of the beginning of thermal oxidative destruction of polyethylene PE-63 is lower as compared to PE-80 and PE-100 (Table 1). The rate of thermal oxidative destruction of polyethylene

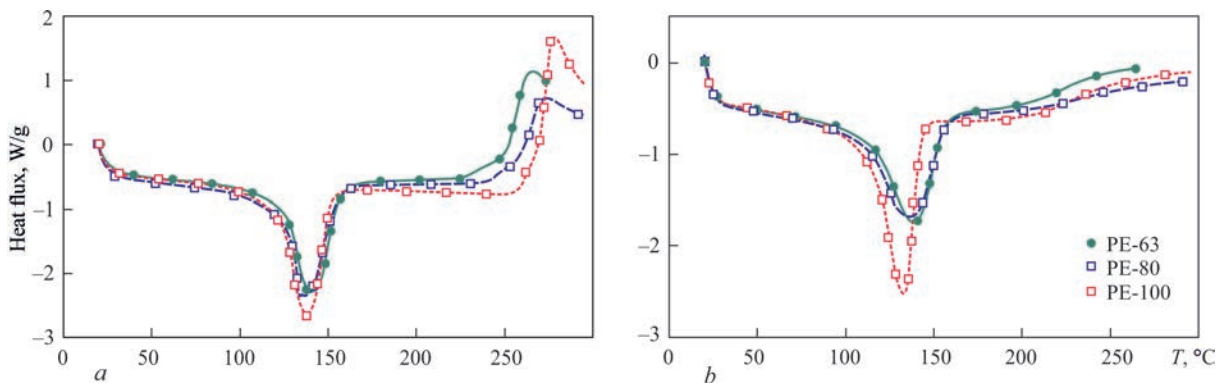


**Figure 3.** DSC curves of specimens of pipe polyethylene grades PE-63, PE-80 and PE-100 during the first (*a*) and second (*b*) heating PE-63 is much higher (Figure 2, *b*) at a temperature of intensity maximum  $T_{d,max} \approx 418$  °C as compared to PE-80 and PE-100 at the temperatures of intensity maxima  $T_{d,max} \approx 420$  and  $450$  °C, respectively.

The corresponding curves were obtained applying the DSC method for the specimens of technical polyethylenes PE-63, PE-80 and PE-100 during the first (Figure 3, *a*) and second (Figure 3, *b*) heating. During the first heating, exothermic processes on the curves at a region of about 250 °C are seen, which are absent during the second heating, which may be associated with thermal relaxation of stresses remaining in the polymer after pipe formation or during a final polymerization of polyethylenes. During the second heating, the change in the character of maxima of en-

dothermic processes in the region of temperatures of 130–140 °C is observed. Therefore, melting of polyethylenes, shift of their temperatures and a decrease in enthalpy occurs during the first heating.

It should be noted that DSC curves of the first and second heating and characteristic thermophysical parameters of melting (Table 2) differ in some way for all three grades of technical polyethylenes.

The comparison of the thermal conductivity curves (Figure 4) shows that this parameter for all three grades of polyethylenes both according to isothermal values as well as with the changes in temperatures can differ in several times, which can not but affect the melting processes during welding.

The creep and stress relaxation curves of the specimens of three grades of polyethylenes at different temperatures were also compared (Figure 5). If at the temperatures much lower than the melting point of individual polyethylenes the isothermal deformation curves of polyethylenes during creep and stress relaxation are similar, then with an approach to the melting point their behavior differs significantly. For the specimen of polyethylene PE-63, the deformation values are the lowest, which is probably connected with its high viscosity, and the specimen of PE-100 is deformed as an already low-viscosity melt.

Thus, the carried out investigations showed significant differences in the thermophysical characteristics of technical polyethylenes, especially between the polyethylene of grade PE-63 and the polyethylenes

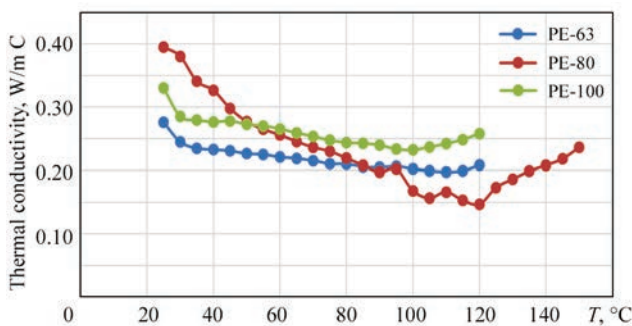


**Figure 4.** Thermal conductivity of technical polyethylenes PE-63, PE-80 and PE-100

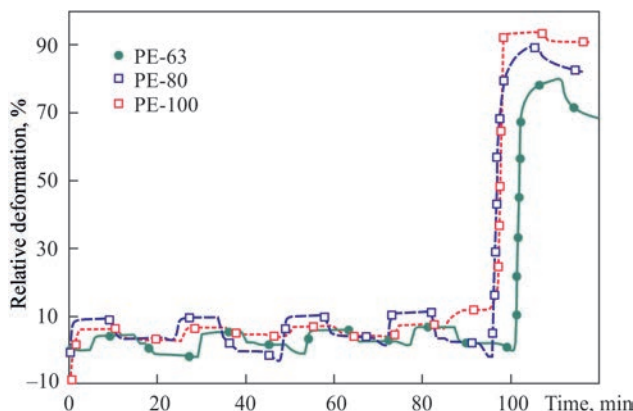


**Figure 5.** Deformation behavior of technical polyethylenes PE-63, PE-80 and PE-100

**Table 2.** Characteristic thermophysical parameters of melting specimens of pipe polyethylenes PE-63, PE-80 and PE-100

Specimen	$T_m$ , °C	$\Delta H$ , J/g
1st heating		
PE-63	141.3	112.0
PE-80	136.9	116.1
PE-100	137.6	120.9
2nd heating		
PE-63	138.9	93.5
PE-80	137.5	95.6
PE-100	133.0	112.3

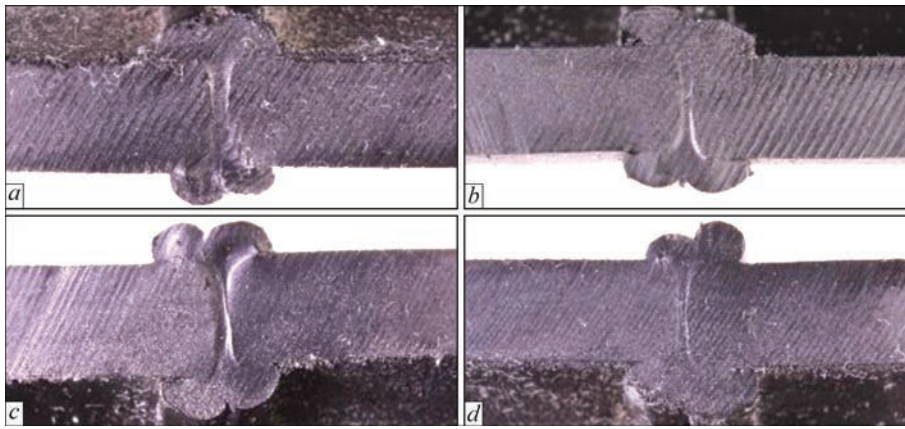


**Figure 6.** Morphology of welded joints of polymer pipes of different- and single-type polyethylenes: *a* — PE-63/PE-63; *b* — PE-100/PE-100; *c* — PE-100/PE-63; *d* — PE-63/PE-80

of grades PE-80 and PE-100. These differences, of course, should be taken into account while welding pipes of different grades of polyethylene. However, the flowchart of the conventional method of butt welding of polymer pipes using a heated tool does not take into account these features.

#### Results of investigations of experimental welds.

In a year after laying into the experimental environment, a study of the morphology and mechanical characteristics of experimental welded joints was carried out. Sections of welds of pipes from the single- and different-type polyethylenes are presented in Figure 6.

There was a significant difference in the shape and volume of the welded flash was revealed in the welded joints on the side of different-type polyethylenes (Figure 6, *c*, *d*) as compared to the welded joints of single-type polyethylenes (Figure 6, *a*, *b*). It is important to note that according to the valid standards [7], the flash of such shape is characteristic of poor quality welded joints, and the welded joint itself is considered

to be unsuitable for use. According to the valid standards for a high-quality weld, the flash beads on both sides of the welding plane should have the same shape and volume, as is seen in welded joints of pipes of single-type polyethylenes. In the case of welded joints of pipes of different-type polyethylenes, a nonuniformly distributed flash is observed on both sides of the welding plane, and therefore, such welded joints may be considered as poor. The difference in the shape and volume of the flash for different-type welded joints is predetermined by the difference in their thermophysical characteristics, which was shown above.

The structure and properties of welded joints of pipes of different-type polyethylenes, which for 2 years were exposed to the action of climatic factors, were studied using an X-ray diffractometer. The analysis of wide-angle X-ray diffraction patterns of the specimens of welded joints PE-63/PE-100, which were in the air and on the ground showed that they all have an amorphous-crystalline structure, which is indicated by the presence of diffraction maxima at  $2\theta_{\max} = 21.2$  and  $23.6$  against the background of an imaginary amorphous halo with an apex at  $2\theta_{\max} \approx 21.0^\circ$  (Figure 7).

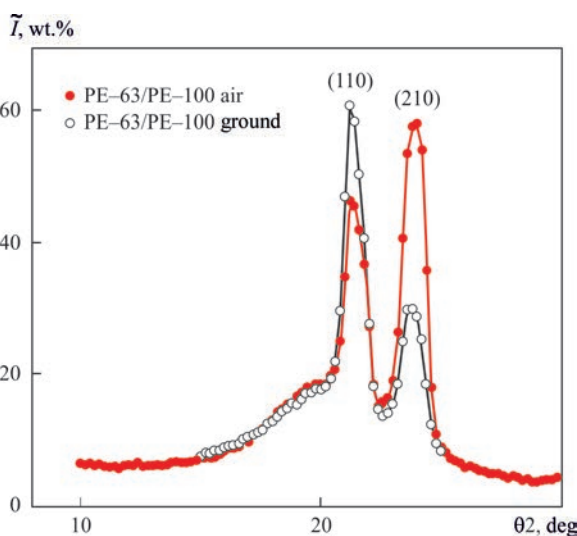


**Figure 7.** Wide-angle X-ray diffraction patterns of welded joints of polyethylenes PE-63/PE-100, which were in the air and on the ground

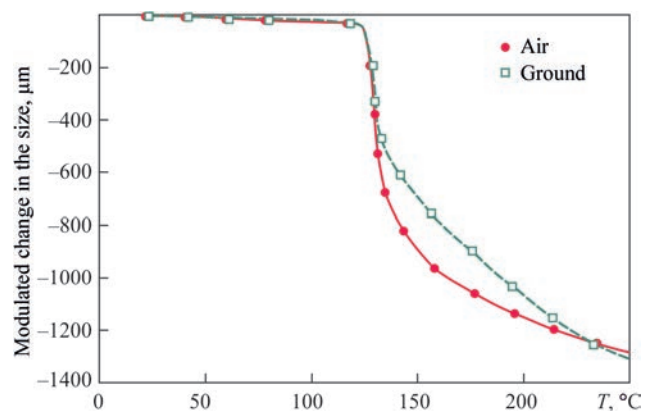


**Figure 8.** Modulated change of the size of specimens of welded joints of PE-63/PE-100, which were under the influence of factors of the operating environment, on temperature

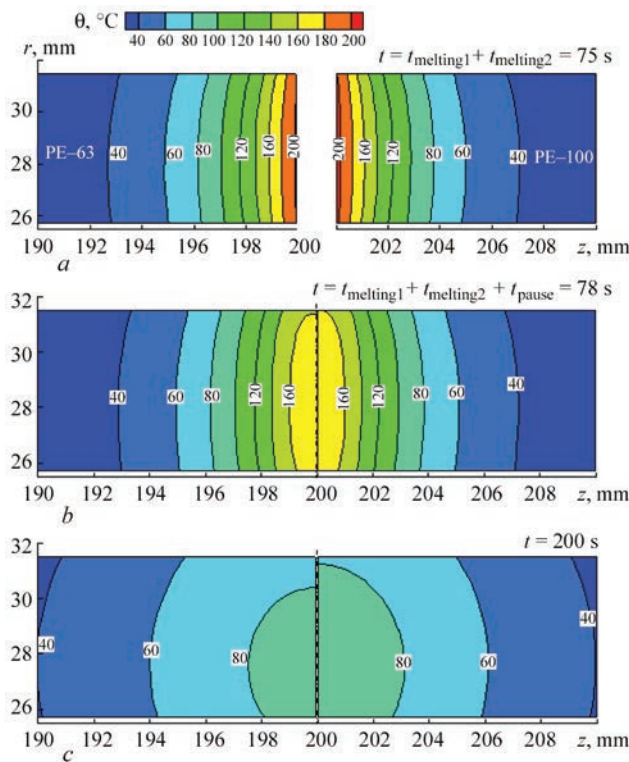


**Figure 9.** Isolines of temperature field at different time points during butt welding of pipes PE-63/PE-100 (see description a–c in the text)

It is noteworthy that for the welded joints of PE-63/PE-100, which were in the air under the action of ultraviolet radiation, a change in the intensity of diffraction maxima in the planes (110) and (200) occurs, which indicates significant changes in the structure of the welded joint material. During the analysis of wide-angle X-ray diffraction patterns of the specimens of welded joints of PE-63/PE-63 and PE-63/PE-80, which were in the air and on the ground, significant changes in their structure organization were not revealed.

Figure 8 shows the curves of the modulated change in the size of the specimens of welded joints of PE-63/PE-100, respectively, which were exposed to the influence of factors of the working environment, from temperature.

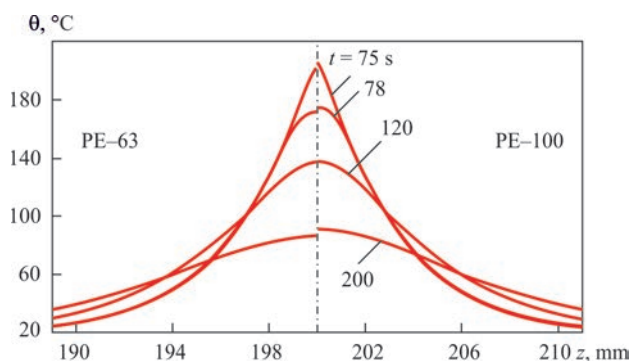


**Figure 10.** Temperature distribution along the midline for different time points during butt welding of pipes PE-63/PE-100

With the exception of an increase in the value of thermal expansion before melting of the crystalline phase of polyethylenes in the specimen of welded joint of PE-63/PE-80, which was on the surface, and a somewhat sharp process of melting the specimen of welded joint of PE-63/PE-80, which was on the ground, a significant difference between the behavior of the thermomechanical curves of both specimens is not observed. This is most likely explained by the absence of significant changes in the structure of both welds. A completely different situation is observed for the specimens of welded joints of PE-63/PE-100. The curves of the modulated change in the size of the specimens of welded joints of PE-63/PE-100, which were exposed to the influence of factors of the working environment, on temperature namely on the surface and on the ground, have a significant difference in the region of melting crystalline phase of polyethylenes. This can certainly be explained by the change in the structure of the crystalline phase of polyethylenes in the weld, which is confirmed by the results of X-ray structural examinations, which are shown in Figure 9.

The service properties of welded joints were studied in the course of mechanical tests in the mode of uniaxial tension (Table 3). It is seen that welded joints of PE-63/PE-80 has the most significant effect on the deterioration of mechanical properties, regardless of the environment. However, it should be noted that the specimens in the ground underwent the major changes in mechanical strength. This is probably associated with the lack of action of ultraviolet radiation, which, as is known, firstly leads to the cross-linking of polyethylene, accompanied by an increase in its strength, against the background of its aging, which to some extent, as is seen from Table, is typical for all specimens.

**Results of mathematical modeling of temperature fields.** In order to evaluate the influence of the difference in thermophysical characteristics of the material on the process of welding different-type polyethylenes, mathematical modeling of temperature fields was performed during the welding process.

Figure 9 shows the isolines of the temperature field at three moments of the butt welding process: a — at the beginning of the technological pause of 75 s;

**Table 3.** Change in mechanical strength of welded joints specimens over time

Specimen	PE-63	PE-80	PE-100
	1 year/2 years	1 year/2 years	1 year/2 years
Ground			
PE-63	19.38/19.68	18.76/18.03	19.69/18.79
Air			
PE-63	19.23/19.48	17.84/16.5	19.53/19.55

**Table 4.** Recommended temperature of operating surfaces of double zone heater during welding of different-type polyethylenes

Temperature of surrounding air, °C	Combinations type of polyethylenes					
	PE-63	PE-80	PE-63	PE-100	PE-80	PE-100
-10-0	230	220	220	230	220	230
0-20	220	210	210	220	210	220
20-45	210	200	200	210	200	210

*b* — at the time of joining of the ends and the beginning of compression of the pipes during upsetting; *c* — approximately in the middle of cooling duration. Because to differences in the thermophysical properties of polyethylenes on different sides of the pipe butt joint, nonuniform thermal fields are formed. In Figure 10 a gradual equalization of temperature in the middle side surface of the pipe is seen.

#### Designing and testing of two-zone heating tool.

The abovementioned investigations of the difference in properties of technical polyethylenes PE-63, PE-80 and PE-100 showed that the use of the conventional scheme of butt welding of different-type pipe polyethylenes using a single-zone heated tool leads to a technologically incorrect weld formation, which according to the nature of the welding process and the appearance of the welded flash does not meet the valid building standards, and therefore a need appeared to create special equipment to provide a quality welded joint during butt welding using a heated tool. To solve the problem of increasing the efficiency of repair and extending the life of plastic pipelines, in the course of the work, a two-zone heating tool for butt welding of pipes with an outer diameter of 110 mm from different-type polyethylenes of pipe grades PE-63 and PE-80, PE-100 using a heated tool was designed and created.

At a regulated heating at different temperature, on the surfaces of a two-zone heater on the ends of pipes on both sides the same quantity of melt is formed, during upsetting the symmetrical weld with the identical sizes of beads of a flash around the whole orbit of a butt is formed.

The conclusion about the mechanical strength of the weld of different-type polyethylene pipes, produced with the help of a two-zone heating tool, is provided by destructive tensile tests of the specimens carried out in accordance with the requirements of the standard DSTU EN12814-2: 2018 [8].

The fracture of the specimens had the similar plastic nature. During plastic deformation of the specimen, the «neck» was formed in the region of the fusion line and propagated towards the less strength polymeric material. The maximum tensile load for the

specimen of PE-80/PE-63 (No.1), welded using the conventional technology, was 710 N, and for the specimen of PE-80/PE-63 (No. 2), welded using the two-zone heated tool, was 880 N. After the corresponding calculations, the yield strength value of the polymeric material was obtained — 25.8 MPa for the specimen No.1 and 29.4 MPa for the specimen No.2. Thus, the strength of the welded joint of different-type polyethylene pipes welded applying the new technology appears to be by 15 % higher. Since the specimens with a narrowed working part were tested, in this case the strength of the weld material was determined. According to the results of experimental studies, the recommended values of temperature on the surfaces of the two-zone heating tool in different environmental conditions were determined (Table 4).

#### Conclusions

In the work the influence of heterogeneity of polyethylenes on the process of their welded joint formation was investigated. The solution to the problem of welding pipes from different-type polyethylenes applying the two-zone heating tool for butt welding using the heated tool created within the framework of this study is given. The technological approaches were developed, that allow producing high-quality welded joints of different-type polyethylenes.

1. Kimelblat, V.I., Volkov, I.V., Glukhov, V.V. (2020) Optimization of resistance butt welding. Accounting for the properties of polymers. *Polimernye Truby*, 28(2), 32–36 [in Russian].
2. Komarov, G.V. (2015) Composition and properties of polymer materials affecting their weldability. *Polimernye Materialy*, 9, 44–48 [in Russian].
3. *GOST 16338–85*: Low-pressure polyethylene. Specifications [in Russian].
4. *GOST R 50838–95*: Polyethylene pipes for gas pipelines. Specifications [in Russian].
5. *DSTU B V. 2.7-73–98*: Polyethylene pipes for the supply of gaseous fuel. Specifications [in Ukrainian].
6. *DSTU B V.2.7-151:2008*: Polyethylene pipes for the supply of cold water. Specifications [in Ukrainian].
7. *DBN V. 2.5–41:2009*: Gas pipelines from polyethylene pipes. Design. Construction [in Ukrainian].
8. *DSTU EN12814–2:2018*: Testing of welded joints of thermoplastics semi-finished products. Pt 2: Tensile test [in Ukrainian].

Received 13.10.2020

# INSIDE WELDS: ADVANCED CHARACTERIZATION OF RESIDUAL STRESSES BY NEUTRON DIFFRACTION

**M. Rogante**

Rogante Engineering Office

Contrada San Michele n. 61, 62012 Civitanova Marche, Italy. E-mail: [main@roganteengineering.it](mailto:main@roganteengineering.it)

Welding processes involve often very high temperature gradients, which can induce elevated residual stresses (RS). It is essential, therefore, to know these RS, especially by determining them experimentally e.g. before and after thermal treatments. Neutron beam techniques contribute in general to the solution of important questions and problems related to the methodological restrictions of the analysis systems normally used: complementary to these investigation methods, they provide concrete and fundamental help to optimize the finished industrial product and increase its performance. Neutron diffraction, in particular, is a powerful tool to assess in a non destructive and non invasive way the RS status in materials and components of technological interest. In this paper, the basic theoretical aspects and some examples are reported, regarding the possible determination of RS by using neutron diffraction in different kinds of welded structures. 39 Ref., 7 Figures.

*Keywords:* residual stress, neutron diffraction, welded joints, advanced characterization

In diverse industrial sectors involving welded joints, the requirements to rise materials and products performances, correspond with market needs and protect more and more public safety and environment, make pressure for continuous innovation and technological adaptations.

During the welding process, steep temperature gradients occur, generating thermal stresses large enough to produce plastic deformation as shape misfits between dissimilar regions of the joint's material. Phase transformations at different times in different locations of the joint can be also induced. From these non-uniformities in temperature, very significant RS — usually, large tensile residual macrostresses (RMS), sometimes of the order of magnitude of yield strength of the materials being joined — can be developed in solidification. Since RS are the stresses occurring in the non-existence of any external load or force (excluding the gravity), they must balance to zero within a component, stresses of one sign being equalized by stresses of opposite sign elsewhere. Surface

RS, in particular, can be either tensile or compressive, depending on size and sign of the volume change with transformation. As the welded material solidifies due to the involved temperature gradient, it cools and begins to contract. The fluid in unsolidified regions cannot support stresses and accommodates the contracting surrounding areas. When this material later solidifies, it will try to contract more than the cooler zones around it, leading to RS, as schematized in a general sense in Figure 1.

RMS in welding also lead to problems of distortion and dimensional control in components [1]. Significant levels of RS are developed, in particular, in the production of thick-section steel welds [2]. Intercrystalline and intergranular stress corrosion cracks, e.g., can occur in tanks and pipeline narrow welded zones, and they are due to the RS produced by the construction technique, and to the presence of aggressive elements [3]. It is of primary importance, therefore, to be able to determine experimentally these stresses and their eventual relaxation following heat treatments, assumed that calculation techniques, such as those based on the finite element method (FEM), are not fully reliable in all cases. These simulation models, actually, miss important information on the real state of the material before and after the welding process, particularly concerning internal RS and nano(micro) structural characteristics that influence remarkably on mechanical features and behaviour of welded joints. The creation of FEM to forecast RS in welded joints is very arduous deprived of evidence from direct measurements. Similar problems are found in other types of assembly, in which gradients of certain critical physical parameters are even higher.

Knowledge of the real performing conditions of welded joints and the effect on material behaviour due to RS and other nano(micro)structural factors should

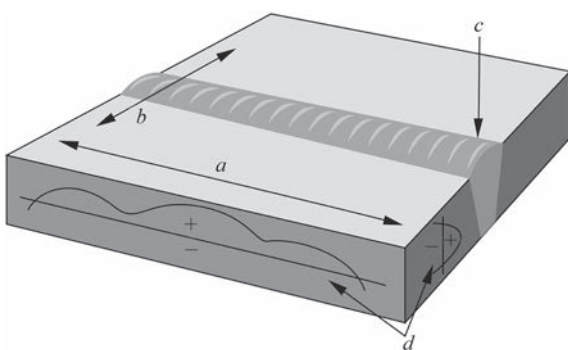


**Figure 1.** RS induced by welding: *a* — longitudinal shrinkage; *b* — transverse shrinkage; *c* — weld seam; *d* — stresses

M. Rogante — <https://orcid.org/0000-0002-6846-0826>

© M. Rogante, 2020

play a crucial role also in the planning phase of a welding process and in the debugging of new welding project methods [4].

Various techniques exist to determine RS but few of them offer the capability to assess completely the RS spatial distribution through the thickness. If the stress distribution does not change (constantly along the welded seam), RS must conform the equilibrium relation:

$$\int_A \sigma_{ij} dA = 0, \quad (1)$$

where  $A$  is the area over which the stresses will balance to zero. The smallest dimensions of this area define a characteristic length which can be adopted to delineate different types of RS. Since RMS are those that balance to zero when integrated over a cross section of a component, the characteristic length for RMS is on the order of the component's dimensions [1].

Some analytical and experimental methods determining RS in welded joints can provide good knowledge and understanding of the effects of component geometry (e.g., concerning thin welded joints, see [5–7]), welding process, thermal and mechanical properties, phase changes and transformation plasticity on the magnitudes and distributions of these RS. This can help studying the RS role in failure mechanisms, improving the existing techniques for reducing RS in sensitive locations and preparing standardised RS profiles useful to calculate the acceptability of defects in welded structures [8, 9].

Refined numerical modelling techniques are generally adopted, particularly in nuclear applications [10], to reproduce the welding process and to model the RS rise during welding, after post weld heat treatment (PWHT), after proof testing and in service under normal and abnormal operating conditions. Despite numerical modelling is a powerful instrument for RS calculation, also in this field of application a validation with reference to experimental results is essential [11].

Neutron beam techniques (NBT) are gaining more and more interest in industrial research and component diagnostics. Among the principal advantages, we can mention their non-destructive and non-invasive character and the possibility to investigate relative massive samples and components, due to the high penetration power of neutrons (order of centimeters in various engineering materials), as compared to other kinds of radiation (e.g., X-rays). Concerning the maximum sample dimensions for measurement in laboratory conditions, they depend on the neutron instrumentation being employed: one of the largest industrial component already investigated by ND, e.g., is the NiCrMoV wheel of an axial compressor for a heavy-duty gas turbine, having a diameter of 482 mm and thickness of 86 mm [12].

NBT results, eventually combined with simulation models such as FEM, can help knowing when failure is likely to occur and whether use of different materials and welding processes would produce a part or a

structure that will last longer. NBT can also contribute in completing the database of structural nano(micro) investigations of welded joints and base materials, developing the nanoscopic safety criterion to forecast and prevent possible fracture processes in joints [13, 14].

Neutron diffraction (ND) has been already adopted to study non-destructively the RS profile through welds and joints and in adjacent zones. Nano(micro)structure, texture [15] and RS analysis can be studied in general by ND, and dedicated diffractometers are continuously developed involving a careful selection and optimization of the diverse mechanical and optical parts, based on intensive examination of the respective purposes.

**Neutron diffraction.** Diffraction methods allow measuring both RMS and microstresses in crystalline materials, since each phase will have its own diffraction pattern supplying information on the stresses in that phase. Using ND to evaluate interplanar spacings in diverse directions, the complete strain tensor may be determined [16]. The main characteristics of ND measurements are:

- determination of the elastic strains only and of one component of the elastic strain tensor by each single measurement;
- strains can be converted to stresses using appropriate elastic moduli;
- selective determination only from grains which are suitably oriented with respect to the scattering vector;
- strain values are averaged over those grains.

In the typical scheme of a strain measurement, a collimated neutron beam with a wavelength  $\lambda$  is diffracted by a polycrystalline sample, then it passes through a second collimator and reaches the detector. Both collimators slits define the investigated volume (see Figure 2), whose cross section, generally, can be as small till  $1 \times 1 \text{ mm}^2$  or, in singular cases, smaller.

Neutron diffractometers (strain scanners) have in general two axes and include: a wavelength selection system (e.g., a bent perfect crystal focusing monochromator), a system of slits allowing sample volume to be estimated; an Euler's cradle, enabling different orientations of the sample and connected to an automated travelling table  $xyz$  allowing for sample positioning; a neutron multidetector or position sensitive detector, which isolates and localises neutron signals on a line or surface, allowing the full diffraction peak to be directly recorded at a certain angular interval; eventual auxiliary equipment to heat up and/or to stress the investigated sample. The resolution of these scanners derived from the full width at half maximum (FWHM) of the diffraction lines, nevertheless, is adequately high for small sample gauge volumes (when the width of the irradiated part of the sample is about 2 mm or less) but rarely better than  $8 \cdot 10^{-3}$  for bulk samples, hence they are adopted to measure the elastic strain effects due to the variations of lattice constants and angular shifts of the diffraction lines. To

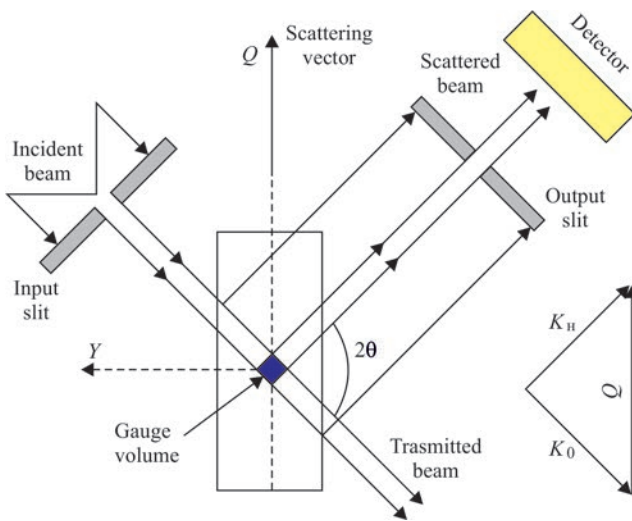


**Figure 2.** General scheme of a strain measurement by neutron diffraction

analyse micro-strain effects resulting in a change of the FWHM and shape of broadened diffraction profiles, a significantly higher resolution is needed which can be achieved just by a 3-axis diffraction set-up recently proposed [17].

Concerning RS calculation, the Bragg law:

$$n\lambda = 2d_{hkl} \sin \theta, \quad (2)$$

(where the integer  $n$  is the diffraction order;  $2\theta$  is the ample take-off angle related to the maximum of the Bragg diffracted intensity peak,  $hkl$  are the Miller indices of the investigated lattice planes) allows calculating the lattice spacing  $d_{hkl}$ . The corresponding lattice strain is given by the relation:

$$\varepsilon_{hkl} = \frac{d_{hkl} - d_{0,hkl}}{d_{0,hkl}} = \frac{\Delta d_{hkl}}{d_{0,hkl}} = -\cot \theta_{hkl} \Delta \theta_{hkl}, \quad (3)$$

where  $\theta_{hkl}$  is the diffraction angle and  $d_{0,hkl}$  is the lattice spacing in a stress-free reference material. As the assessment of RS by ND is always related to the stress-free material state, a correct evaluation of the unstressed lattice parameters (e.g., the interplanar distance) is one of the key tasks, in order to avoid improper errors during the real material strain and stress evaluation. The accessibility of carefully measured zero-strain standards is also essential to confirm the absence of methodical instrumental effects determining the diffraction profile at a chosen scattering angle. The stress-free particular, Some efforts are under way, hence, to develop new methods allowing more and more precise and practical evaluations of the unstressed lattice parameters, hence of the residual strains and stresses [18, 19]. Furthermore, at welding structural steels, phase microstructural transformations undergo in the fusion zone and in the HAZ. Each phase possesses its own lattice spacing and it is not known in advance in what volume the phase transformations have occurred. In ND measurements, hence, the microstructural phase composition, distributed

non uniformly in the volume of welded joint metal should be taken into account.

The RS values can be obtained, in general, by knowing the elastic constants of the considered material and using the relations:

$$\begin{aligned} \sigma_{xx} &= \frac{E}{(1+\nu)(1-2\nu)}(1-\nu)\varepsilon_{xx} + \nu(\varepsilon_{yy} + \varepsilon_{zz}); \\ \sigma_{yy} &= \frac{E}{(1+\nu)(1-2\nu)}(1-\nu)\varepsilon_{yy} + \nu(\varepsilon_{xx} + \varepsilon_{zz}); \\ \sigma_{zz} &= \frac{E}{(1+\nu)(1-2\nu)}(1-\nu)\varepsilon_{zz} + \nu(\varepsilon_{yy} + \varepsilon_{xx}), \end{aligned} \quad (4)$$

where  $\sigma_{xx}$ ,  $\sigma_{yy}$  and  $\sigma_{zz}$  are the principal stresses;  $E$  is the Young's modulus and  $\nu$  is the Poisson's ratio in an elastically isotropic model.

Uniaxial or biaxial RS are usually determined by ND as standard, and by rotating the triaxial component (4) RS can be determined with nominal accuracies of about  $\pm 30$  MPa (e.g., in steel) and  $\pm 10$  MPa (e.g., in aluminium).

In a ND analysis to determine RS, finally, peak shifts not associated to strain changes — i.e., pseudo peak-shifts or pseudo strains — should be avoided or corrected, as well as errors and uncertainties for measurements near surfaces eventually created by beam optics. Many possible systematic effects, indeed, may affect the interpretation of of ND data. For a full treatment of the theoretical bases, see ref. [1, 12, 16, 18–21].

**Some application in the welding sector.** Among the examples of application of ND to determine the RS profile, the following cases can be mentioned [22]:

- double-V welds — see, e.g., the analysis of a 50D C-Mn steel sample having dimensions of 13.5×240×42 mm ( $x, y, z$ ), using the Bragg reflection (211), obtaining RS values along the  $y$  and  $z$  directions determined as function of coordinate  $z$ , in good agreement with conventional destructive method (strain gauge rosette);

- $T$  weld — see, e.g., the analysis of a steel part from the offshore industry, in which deformation measurements in three directions were carried out for two series of point, confirming, as expected, the further away from the weld, the smaller the deformations;

- $V$  welds — see, e.g., the analysis of an AISI 303 stainless steel part, with an investigated volume of 2.5×2.5×200 mm, using the (111) reflection to draw a deformation map.

RS measurements by ND have been performed before and after relaxation heat treatment in a 2.25Cr1Mo ferritic steel arc welded pipe adopted for heat exchangers, having the following dimensions (mm): outside diameter = 218; internal diameter = 178; total length = 355. The 2.25 Cr1Mo steel is one of the most extensively used and best characterised grade among the chrome-molybdenum steels: it is generally used in steam generators and it is often preferred to austenitic steels, since its reduced weldability problems. Exercise

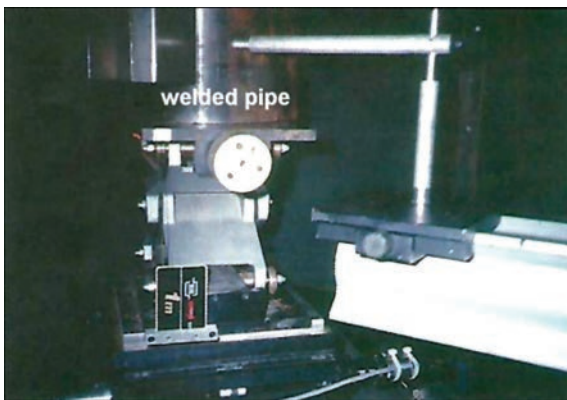


**Figure 3.** 2.25Cr1Mo ferritic steel arc welded pipe positioned at the neutron diffractometer during the ND investigation (Image credit: Rogante Engineering Office)

temperature and pressure ranges are respectively 350–540 °C and 100–200 bar. Points of the pipe have been investigated at the following depth (mm): 2.5; 5; 7.5; 10. Figure 3 shows the considered welded pipe during the analysis.

Figure 4 represents hoop RS before and after the relaxation heat treatment (5 mm depth).

The gap between the RS values self-explains the resulting deviation trend between heat treated and not heat treated material [23]. An asymmetric progression of RS appeared across the welding: values shifted in high passing from one hand to the other of the weld zone, following the passes direction. Such trend can be ascribed to the asymmetry of the welding process, scheduling in the fibre the latest to cool a greater tensional level in comparison with the adjacent regions. RS after the heat treatment appear nothing along the radial direction, while along the axial one they are lower than before the heat treatment, exhibiting a mono-dimensional status [24].

Two 2.25Cr1Mo butt welded steel plates (A and B) have been investigated by ND before and after welding by shielding metal arc. Strain measurements have been performed in the plate A (before welding) along the three main directions  $x$ ,  $y$  and  $z$ , in 11 aligned points inside the material, at the following depths (mm): 6.25, 12.5 and 18.75. Low tensile RS (<100 MPa) resulted in each direction. From strain measurements carried out in two points of Plate B near the calking, low tensile (40 MPa) and very low compressive (–10 MPa) RS have been found, perpendicular and parallel to the calking respectively, uniform through the thickness. Post welding RS resulted to change their trend close to the weld bead, and a symmetrical behaviour has been observed in  $x$  and  $y$  RS components at the depths of 6.25 mm and 18.75 mm. In correspondence of the middle thickness (12.5 mm), the effect of welding on the RS field appeared lower, as compared with other depths. Analogous trends have been found for the  $z$  RS component. Results obtained by ND have shown a good agreement for two measured points in compar-

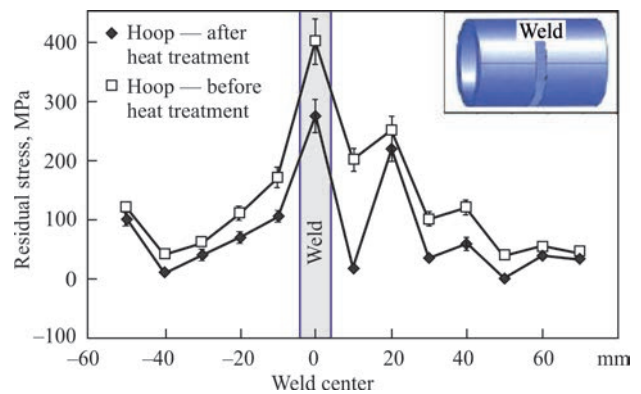


**Figure 4.** Hoop RS (5 mm depth) determined by ND in a 2.25Cr1Mo ferritic arc welded pipe before and after relaxation heat treatment

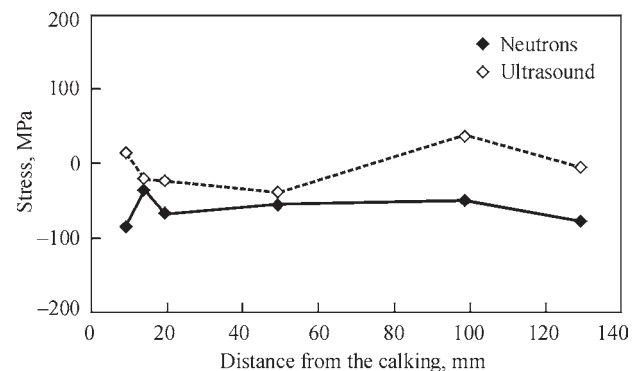
ison with data from ultrasonic testing (UT) averaged through the whole thickness (see Figure 5) [25].

Figure 6 is referred to the determination of residual micro-strains by ND in a pipe-flange welded joint made of steel.

A  $2 \times 2 \times 5$  mm<sup>3</sup> gauge volume was adopted, and the dimensions of the joint were the following (mm): thickness of the pipe wall = 8; diameter of the pipe = 100; thickness of the base = 12 [12].

In the Oil & Gas sector, the consistency of the several welded joints involved in a pipeline and the eventual occurrence of micro-cracks due to the welding processes can favour a yielding of the whole pipeline structure. A correct method to assess RS, in this case, is essential in achieving the desired safety and reliability levels. Knowledge of RS status and other micro-structural factors (e.g., inhomogeneities, micro-voids, precipitates) present in pipelines can help also correcting the processes of selecting pipe manufacturers, specifying quality of materials, establishing safe operating pressures and better planning maintenance and rehabilitation plans. Some components of the combined total stress may exceed a particular design stress limit for the constitutive material of these pipelines, involving, thus, the risk of an early structural failure.

RS, consequently, represents a peculiar problem in pipelines, where their evaluation is usually performed through typical methods such as ultrasonic measure-



**Figure 5.** Through-the-thickness averaged  $\sigma_x - \sigma_y$  RS components determined in a 2.25Cr1Mo butt welded steel plate by ND, compared with data obtained by UT

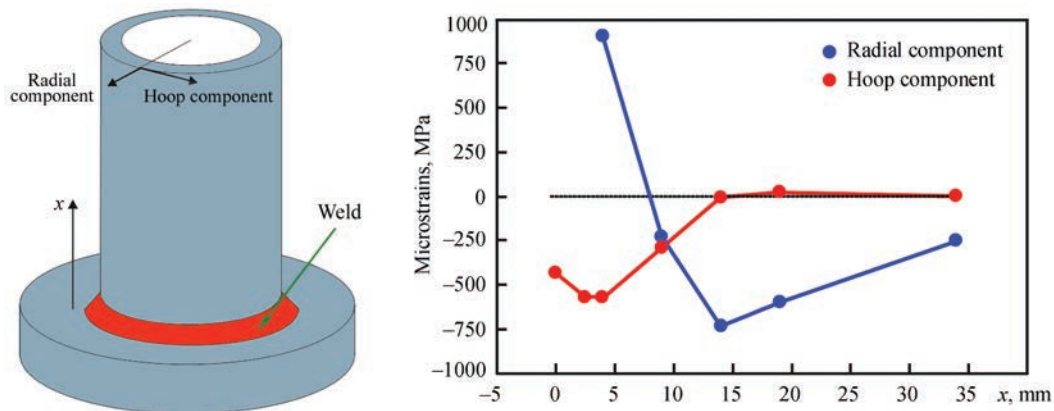


**Figure 6.** Determination of residual strains by ND in a pipe-flange welded joint [12]

ments, magnetic flux leakage or in-situ direct measurement of absolute levels of biaxial stress in ferromagnetic pipelines, based on magnetic anisotropy and permeability. This evaluation results difficult and incomplete, due to the lack of essential information related to the real state of the involved bulk material, which favours pessimistic estimates and risks of failures.

The correct assessment of RS levels performed by ND allows revealing the hidden cause-effect connections between the current condition of a given pipeline material under study and its potential failure modes under operating conditions. Knowledge of such relationships consents forecasting which types of failure modes are likely to occur and the pipeline material resistance to crack propagation under operating conditions.

A feasibility study has been carried out by the Rogante Engineering Office (REO) on the determination of RS in pipelines. A failure predictive model has been proposed, in such work, based on nano(micro) scale level investigations and able to penetrate into the design and development procedure of pipelines. This model involves ND, to identify the cost-effective materials minimizing the production of RS, reducing stress-related failures and improving the pipelines reliability. It includes also the planning of a relational database formed by a collection of catalogued material parameters obtained also from ND for fresh samples which represent, statistically, the population of pipelines on which the forecasting tool is intended to

be employed [23, 26]. Concerning the criteria of collecting samples for ND investigation, e.g., suggested dimensions concerning samples from pipe of large external diameter (> 500 mm) are reported in Figure 7.

By cutting the original pipe to obtain the sample, a change occurs of the RS due to manufacture (not due to the welding process); before cutting the sample, consequently, it is necessary to apply extensometers at both the inner and the external surface of the pipe, to check the signal before and after cutting and record the RS alteration. Since thermal cutting of such samples adds heat-affected zone (HAZ) effects, the most adequate and less contaminating cutting procedure is grinding, also involving a cooling medium, to avoid temperatures  $\geq 300$  °C. Samples should be very precisely cut, to possess identical geometry with not more than 2 mm error in the sizes: the time necessary for sample alignment at the neutron instrumentation, consequently, would be reduced.

Another example of possible applications of ND concerns the railway sector, i.e. the determination of inner and sub-surface RS arising in the welds of structural connections of the frame of wagons [27].

A further possible application concerns the welding of steels as constitutive materials of moulds, for their repair. The welding processes usually adopted in this case are manual metal arc welding (MMA), tungsten inert gas welding (TIG), laser beam welding (LBW) and electro-spark deposition (ESD). In planning these processes, it must be taken into account that they generally implicate high temperature gradients from which both undesirable metallurgical modifications in the portions affected by the heat contribution and RS are created. The thermal gradients originating during the shrinkage, in particular, would lead contiguous areas of material to simultaneously assume different lengths, but this is impossible. These zones, to maintain the same length at all times, must therefore be subjected to tensions — compression or traction, depending on the temperature gradient. Critical situations can arise, therefore, with the appearance of fixed deformations and even cracks. The latter can occur in correspondence with both the HAZ and outside that zone. An advanced characteriza-

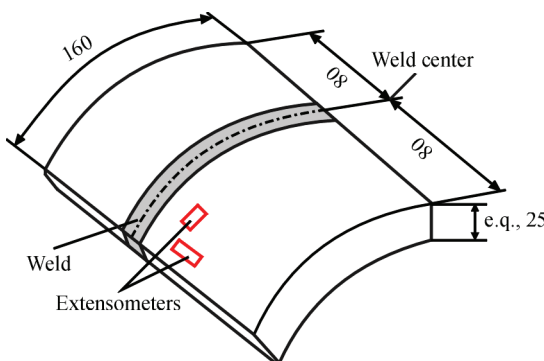


**Figure 7.** Suggested dimensions (mm) of the sample for ND investigation. External diameter of the pipe > 500 mm

tion of such welds by NBT, therefore, can be beneficial since it contemplates the various parameters responsible for performance and quality, including inner and sub-surface RS stresses [28]. Similarly happens for the welding of cast irons [29].

The following other examples can be reported of ND investigation for RS determination: AISI 304 butt welded 28" pipe (two TIG passes, and lastly twenty-six SMA passes distributed on ten layers) [30]; X welded sample (50 D C–Mn steel), a fillet weld of a steel component for offshore applications [31]; Al-2219 welded plate (62×48×6.5 mm) for spacecraft industry [32]; determination of RS longitudinal to electron beam weld in a Ni-based superalloy [33]; electron beam welded Ti-834 plate [34]; an Alloy 600 plate filled with three Alloy 82 weld beads, simulating a repair weld, in the frame of an international measurement round robin on an Alloy 600/82 multi-pass weldment [35]; near surface and inner RS around the weld toe of Weldox 1300 plates with a thickness of 15 mm, joined by robotic gas metal arc welding (GMAW) with Ar + 18 % CO<sub>2</sub> as shielding gas [36]; fillet welds in 8 mm 900 MPa steel, with RS mapping perpendicular and parallel to the weld line and through the thickness in the vicinity of weld toe position [37]; bead-on-plate weldment, showing the significance of the weld start and end sites on the residual strain/stress distribution [38]; a rolled joint of a pressure tube made of three axial symmetric parts, modified SUS403 stainless steel as an inner extension, Zr–2.5Nb as the pressure tube and an Inconel 718 outer sleeve, to study the RS relaxation after a short-time aging treatment at 350 °C carried out to simulate thermal aging over the lifetime of an advanced thermal reactor at operating temperature [39].

Further applications concerning RS determination by ND in manual metal arc repair, alumino-thermic and friction-based welds are reported in [20].

## Conclusion

A huge amount of work has been performed on the field of welded joints and materials weldability, to solve standard issues present in welding manufacturing [4]. The increase of the investigation in welds is fundamental to develop a correct design and weldment performance, with the main aim to improve strategies for prolonging component and plant lifetime.

The ND method is of great interest to specialists in welding, since it allows determining the distribution of RS over the thickness of different types of structural elements. There are high potentials that the ND method will make it possible to determine the complex RS state, which is formed during multipass welding of thick-walled elements made of steels with structural phase transformations. ND, indeed, has shown to be a valuable tool both to advance new joining processes and to enhance more traditional techniques. This method is also capable to validate FEM adopted for weld process optimization, to study in-situ post-weld

heat treatments and to analyse the result of phase transformations during welding.

Since the thermal treatment due to the welding process influences also the nano(micro)structure, moreover producing the growth of some inclusions (e.g., precipitates), another NBT, i.e. small angle neutron scattering (SANS), is indicated to complete the analysis of welded joints: by knowing their chemical nature, it allows obtaining key characteristics of these defects (e.g., number and size distribution).

For industrial applications of NBT, the REO has long been developing dedicated methodological approaches with appropriate processing and treatment procedures of data from neutron measurements, including those for RS assessment in welding.

**Acknowledgements.** Dr. O. Makhnenko and Dr. A. Zavadovev are acknowledged for useful discussions.

1. Winholtz, R.A., Rogante, M. (2016) Residual stresses: Macro- and microstresses. *Reference Module in Materials Science and Materials Engineering*, 1–5. Elsevier, Oxford. <https://doi.org/10.1016/B978-0-12-803581-8.03038-1>
2. Smith, D.J., Bouchard, P.J., George, D. Measurement and prediction of residual stresses in thick-section steel welds. *The J. of Strain Analysis for Engineering Design*, 35(4), 287–305. <https://doi.org/10.1243/0309324001514422>
3. Rogante, M., Battistella, P., Cesari, F. (2006) Hydrogen interaction and stress-corrosion in hydrocarbon storage vessels and pipelines welding. *Int. J. of Hydrogen Energy*, 31(5), 597–601. <https://doi.org/10.1016/j.ijhydene.2005.05.011>
4. Rogante, M., Lebedev, V.T., Kralj, S. et al. (2006) Neutron techniques for welding project methods development in nuclear/traditional industrial application. *Multidiscipline Modeling in Materials and Structures*, 2(4), 419–433. <https://doi.org/10.1163/157361106778554824>
5. Rogante, M., Cesari, F.G., Ferrari, G. (2009) Analytical method for residual stresses determination in thin welded joints. *Ibid.*, 5(3), 269–276. <https://doi.org/10.1163/157361109789016998>
6. Rogante, M., Cesari, F.G., Ferrari, G., Battistella, P. (2006) A simplified solution for the evaluation of residual weld stress. *Welding Int.*, 20(9), 713–716. <https://doi.org/10.1533/wint.2006.3635>
7. Cesari, F.G., Ferrari, G., Molinari, V. et al. (2001) A simplified evaluation model of residual stresses distribution in weldings. In: *Proc. of 4<sup>th</sup> Eur. Conf. on Welding, Joining and Cutting «EUROJOIN 4» (Cavtat, Dubrovnik, Croatia, 24–26.05.01)*. Ed. by S. Kralj, Z. Kožuh. Zagreb, Croatia, ISBN/ISSN 953-96454-0-9, 251–256.
8. Stacey, A., Barthelemy, J.Y., Leggatt, R.H., Ainsworth, R.A. (2000) Incorporation of residual stresses into the SINTAP defect assessment procedure. *Engineering Fracture Mechanics*, 67(6), 573–611. [https://doi.org/10.1016/S0013-7944\(00\)00075-8](https://doi.org/10.1016/S0013-7944(00)00075-8)
9. (2019) *Guide to methods for assessing the acceptability of flaws in metallic structures, Report BS 7910:2019, British Standards Institution*. ISBN 9780580520860, p. 535. [https://shop.bsigroup.com/en/ProductDetail/?pid=000000000030369478&\\_ga=2.128792330.701546373.1576593016-1872050251.1562055730](https://shop.bsigroup.com/en/ProductDetail/?pid=000000000030369478&_ga=2.128792330.701546373.1576593016-1872050251.1562055730)
10. Smith, S.D. (1991) *A review of numerical modelling of fusion welding for the prediction of residual stresses and distortion*. TWI Members Report 437/1991. <https://www.twi-global.com/pdfs/industrial-member-reports/437-december.pdf>

11. Rogante, M. (2011) Neutron techniques for developing engineering welding methods. *Welding International*, **25**(10), 754–761. <https://doi.org/10.1080/09507116.2011.581347>
12. Rogante, M. (2008) Applicazioni Industriali delle Tecniche Neutroniche. In: *Proc. of 1<sup>st</sup> Italian Workshop for Industry on Industrial Applications of Neutron Techniques (Civitanova Marche, Italy, 12–14.06.2008)*, 40–120. Ed. by M. Rogante.
13. Lebedev, V.T., Kralj, S., Rogante, M. et al. (2005) Industrial applications of welding project methods: state of the art and development perspectives. In: *Proc. of Int. Conf. on Welding and Joining-2005: Frontiers of Materials Joining (25–28.01.2005, Tel-Aviv, Israel)*, 163–177. Ed. by A. Stern, Vol. ICRA-2005-ISR-23.
14. Lebedev, V.T., Kralj, S., Rogante, M., Rosta, L. (2004) Welded joints project methods for nuclear/traditional industrial applications: the international state-of-the-art. In: *Proc. of 3<sup>rd</sup> Int. Conf. on Welding in Maritime Engineering (Hvar, Croatia, 02–05–06.2004)*, 87–98. Ed. by Z. Kožuh. Croatian Welding Society, Zagreb, Croatia.
15. Rogante, M. (2001) Tessitura e proprietà dei materiali. *Progettare, VNU*, **247**, 72–76. Ed. by B. Cisisello. Milano [in Italian].
16. Noyan, I.C., Cohen, J.B. (1987) *Residual Stress: Measurement by Diffraction and Interpretation*. Springer-Verlag, New York, 276. <https://doi.org/10.1007/978-1-4613-9570-6>
17. Mikula, P., Ryukhtin, V., Rogante, M. (2019) On a possible use of neutron three axis diffractometer for studies of elastic and plastic deformation of polycrystalline materials. In: *Proc. 57<sup>th</sup> Conf. on Experimental Stress Analysis EAN 2019 (Luhačovice, Czech Republic, 3–6 June 2019)*, 286–290. Ed. by J. Petruška et al. Czech Society for Mechanics. Book of Extended Abstracts, 101–102, ISBN 978-80-214-5753-9.
18. Rogante, M. (2000) The stress-free reference sample: the problem of the determination of the interplanar distance  $d_0$ . *Physica B: Condensed Matter*, **276–278**, 202–203. [https://doi.org/10.1016/S0921-4526\(99\)01281-8](https://doi.org/10.1016/S0921-4526(99)01281-8)
19. Rogante, M., Mikula, P., Vrána, M. (2014) Assessment of the unstressed lattice parameters for residual stresses determination by neutron diffraction in engineering materials. *Key Engineering Materials*, **592–593**, 465–468. <https://doi.org/10.4028/www.scientific.net/KEM.592-593.465>
20. Hutchings, M.T., Withers, P.J., Holden, T.M., Lorentzen, T. (2005) *Introduction to the characterization of residual stress by neutron diffraction*, 1<sup>st</sup> Ed. CRC Press, Boca Raton <https://doi.org/10.1201/9780203402818>
21. Rogante, M. (1999) *Caratterizzazione, mediante scattering neutronico, di materiali e componenti per l'impiantistica nucleare ed industrial*. Nuclear Engineering Ph.D., University of Bologna, Italy [in Italian]. <https://opac.bncf.firenze.sbn.it/bncf-prod/resource?uri=TS19902210&v=l&dcnr=4>
22. Albertini, G., Bruno, G., Calbucci, P. et al. (1998) Non-destructive determination of residual stresses in welded components using neutron diffraction. *Welding Int.*, **12**(9), 698–703. <http://dx.doi.org/10.1080/09507119809452037>
23. Rogante, M. (2005) Neutron examination techniques applied to pipelines. *Oil & Gas J.*, Sept. **26**, 59–64. <https://www.ogj.com/drilling-production/production-operations/article/17235734/neutron-examination-techniques-applied-to-pipelines>
24. Rogante, M., Rosta, L. (2005) Nanoscale characterisation by SANS and residual stresses determination by neutron diffraction related to materials and components of technological interest. *Proc. of SPIE*, **5824**, 294–305. <https://doi.org/10.1117/12.606090>
25. Albertini, G., Bruno, G., Fiori, F. et al. (1997) Studies of residual stresses, microstructural evolution and texture in steels and alloys by neutron techniques. In: *Proc. of ECSC Workshop on Modelling of Steel Microstructural Evolution during Thermomechanical Treatment*. Brussels, Belgium, 185–195; ISBN 92-827-9891-7; CG-NA-17585-EN-C.
26. Genta P., Rogante M. (2009) Failure predictive models for pipelines through Neutron Diffraction-based stress assessment tools. *The Open Petroleum Engineering J.*, **2**, 12–16. <http://dx.doi.org/10.2174/1874834101002010012>
27. Rogante, M. (2017) I vantaggi delle tecniche neutroniche: possibili applicazioni nel settore ferroviario. *Tecnologie Meccaniche, DB Information Editore, Milano*, **11**, 153–158 [in Italian].
28. Rogante, M. (2019) Saldatura degli acciai per stampi. *Stampi, Tecniche Nuove, Milano*, **1**, 36–41 [in Italian].
29. Rogante, M. (2017) Saldatura delle ghise: tecnologia e applicazioni, Fonderia Pressofusione. *Ibid.*, **3**, 54–58 [in Italian].
30. Albertini, G., Bruno, G., Carsughi, F. et al. (1996) Neutron large and small angle diffraction techniques in industrial and automotive applications. In: *Proc. of 1<sup>st</sup> Int. Conf. on Control and Diagnostics in Automotive Applications, Genova, 03–04/10/1996*. SGE-Servizi Grafici Editoriali, Padova, ISBN 88-8281-16-1, 155–166. <https://epubs.stfc.ac.uk/work/7544>
31. Albertini, G., Bruno, G., Fiori, F. et al. (1996) Non-destructive determination of residual stresses in materials and weldings by neutron diffraction technique. In: *Proc. of 1<sup>st</sup> Int. Conf. «MATEH 1996 – Development, Testing and Application of Materials»*. Opatija, Croatia, 02–05/10/1996, *Croatian Society for Materials and Tribology, Zagreb*, 187–194. <https://epubs.stfc.ac.uk/work/7540>
32. Albertini, G., Bruno, G., Carradò, A. et al. (1999) Determination of residual stresses in materials and industrial components by neutron diffraction. *Measurement Sci. and Technology*, **10**(3), 56–73. <https://doi.org/10.1088/0957-0233/10/3/006>
33. Withers, P.J., Bhadeshia, H.K.D.H. (2001) Residual stress. Pt 2: Nature and origins. *Mater. Sci. and Technol.*, **17**, 366–375. <https://doi.org/10.1179/026708301101510087>
34. Conlon, K.T., Dye, D., Roggie, R.B., Root, H. (2003) Application of neutron diffraction in materials science and engineering. *Neutron News*, **14**(2), 14–19. <https://doi.org/10.1080/10448630308218713>
35. Akrivos, V., Wimpory, R.C., Hofmann, M. et al. (2020) Neutron diffraction measurements of weld residual stresses in three-pass slot weld (Alloy 600/82) and assessment of the measurement uncertainty. *J. of Applied Crystallography*, **53**, 1181–1194. <https://doi.org/10.1107/S1600576720009140>
36. Harati, E., Karlsson, L., Svensson, L.E. et al. (2017) Neutron diffraction evaluation of near surface residual stresses at welds in 1300 MPA yield strength steel. *Materials*, **10**(6), 593. <https://doi.org/10.3390/ma10060593>
37. Mraz, L., Karlsson, L., Vránam M., Mikula, P. (2014) Residual stress distributions at high strength steel welds prepared by low transformation temperature (LTT) and conventional welding consumables. *Mater. Sci. Forum*, **777**, 40–45. <https://doi.org/10.4028/www.scientific.net/MSF.777.40>
38. Paradowska, A.M., Price, J.W.H., Finlayson, T.R. et al. (2010) Comparison of neutron diffraction measurements of residual stress of steel butt welds with current fitness-for-purpose assessments. *J. of Pressure Vessel Technology*, **132**, 051503. <https://doi.org/10.1115/1.4000344>
39. Hayashi, M., Root, J.H., Rogge, R.B., Xu, P. (2018) Evaluation of residual stress relaxation in a rolled joint by neutron diffraction. *Quantum Beam Sci.*, **2**(4), 21. <https://doi.org/10.3390/qbs2040021>

Received 05.11.2020

# DEVELOPMENT OF THE TECHNOLOGY OF RECONDITIONING THE SEALING ELEMENT OF NOZZLE BLADE SECTOR FROM DIFFICULT-TO-WELD HIGH-TEMPERATURE NICKEL ALLOY OF ZhS6 TYPE BY MICROPLASMA POWDER SURFACING

**K.A. Yushchenko, O.V. Yarovitsyn, O.O. Nakonechnyi,  
I.R. Volosatov, O.O. Fomakin and G.D. Khrushchov**

E.O. Paton Electric Welding Institute of the NAS of Ukraine

11 Kazymyr Malevych Str., 03150, Kyiv, Ukraine. E-mail: office@paton.kiev.ua

In order to ensure the technological strength at reconditioning of the side sealing element of a sector of nozzle blades from ZhS6K alloy with the required deposition volume of 7–13 cm<sup>3</sup>, a less heat-resistant material with sufficient deformability was selected. At microplasma powder surfacing it is characterized by the following level of values of short-time strength relative to the deposited metal ZhS6K: 0.7–0.8 at 20 °C; 0.5–0.55 at 1000 °C. Compared to the known technological solutions based on filler materials of IN625 type, it allowed increasing the level of deposited metal high-temperature strength by practically 2 times at 1000 °C at effective limitation of high-temperature ductility  $\varepsilon_{1000\text{ °C}} \leq 1.0\text{--}1.5\%$ . Proceeding from the described materials science studies, PWI developed a new repair technology of microplasma powder surfacing that has successfully passed experimental-practical trials at SE «Lutsk Repair Plant «Motor». 10 Ref., 2 Tables, 5 Figures.

*Keywords:* high-temperature nickel alloy ZhS6K, microplasma powder surfacing of 7–13 cm<sup>3</sup> volume, deformability, technological strength, short-time strength values, repair technology

It is known [1] that after operation for more than 700 h the relative quantity of damaged parts rises significantly in one of the modern bypass gas turbine engines with an afterburner. A typical representative of such parts is the sector of nozzle blades (SNB) of a high-pressure turbine (HPT) from high-temperature nickel alloy (HTNA) ZhS6K (Figure 1, *a* and Table 1), which belongs to the group of stator parts. One of the main types of operational damage of this SNB are thermal fatigue cracks, making it impossible to apply the currently available reconditioning technologies using methods based on fusion welding and brazing, (Figure 1, *b*) and loss or damage of the design shape of a large number of sections of the side sealing element, as a result of corrosion-erosion damage at high temperatures (Figure 1, *c*). Cutting out such defects requires practically complete removal of the material of HPT SNB side sealing element (Figure 1, *d*).

Design-technological analysis of a typical repair cutting out of HPT SNB side sealing element (Figure 2, *a*, *b*) showed the need for deposition of large volumes of HTNA —  $v_d = 7\text{--}13\text{ cm}^3$ , depending on the number of its damaged sections. Use of IN625 type alloys without dispersion strengthening by  $\gamma'$ -phase as the deposited metal for the side sealing element (see Table 1) for this SNB was considered unpractical, because of the risk of losing the spatial stability of the reconditioned structural element as a result of a reduced high-temperature strength and increased ductility of such a material in operation at  $T \geq 1000\text{ °C}$ . It should be noted that the authors of this work are unaware of any previous examples of application of repair technologies of aviation GTE parts with such an increase of the volume of deposition of HTNA with a high content of strengthening  $\gamma'$ -phase. Analysis of publications in the post-Soviet space showed

**Table 1.** Content of the main alloying elements in nickel alloys ZhS6K and IN625, wt.%

Alloy	C	Cr	Ni	Co	Al	Ti	Mo	W	Nb	Ta	Re	Fe	B
ZhS6K	0.13–0.2	9.5–12.0	Base	4.0–5.5	5.0–6.0	2.5–3.2	3.5–4.8	4.5–5.5	1.4–1.8	<2.0	<0.4	<0.4	<0.02
IN625	0.10 max	20.0–23.0	Same	1.0 max	0.4 max	0.4 max	8.0–10.0	–	3.15–4.15	–	–	5.0 max	–

K.A. Yushchenko — <https://orcid.org/0000-0002-6276-7843>, O.V. Yarovitsyn — <https://orcid.org/0000-0001-9922-3877>, O.O. Nakonechnyi — <https://orcid.org/0000-0002-6098-0413>, I.R. Volosatov — <https://orcid.org/0000-0003-2593-9869>, O.O. Fomakin — <https://orcid.org/0000-0001-8903-3340>, G.D. Khrushchov — <https://orcid.org/0000-0002-4045-3587>

© K.A. Yushchenko, O.V. Yarovitsyn, O.O. Nakonechnyi, I.R. Volosatov, O.O. Fomakin and G.D. Khrushchov, 2020

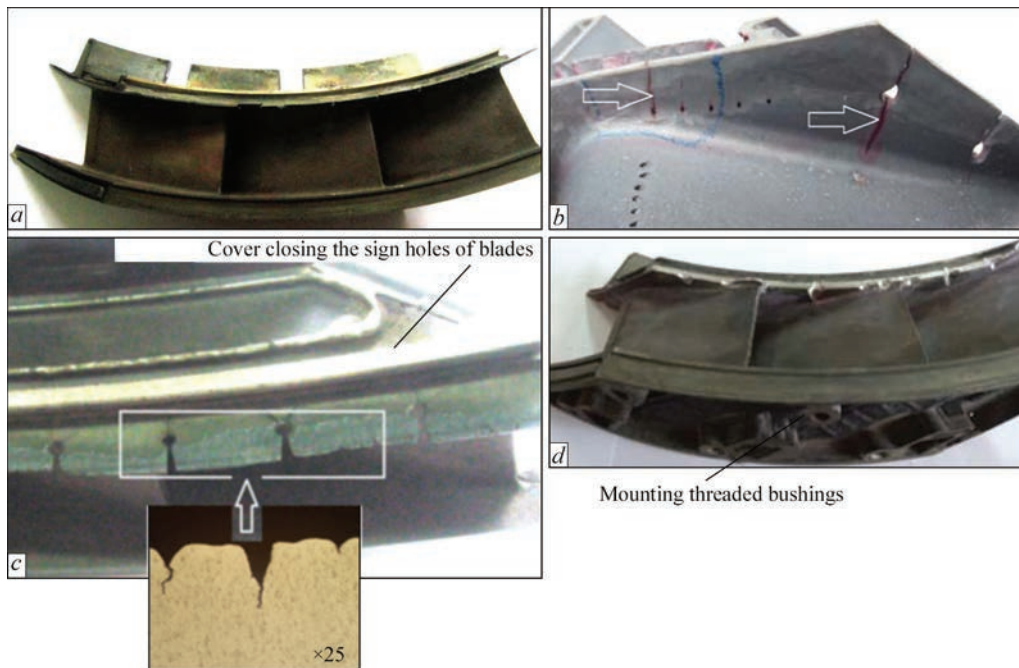


**Figure 1.** Appearance of HPT SNB from ZhS6K alloy (a), its operating damage (b, c) and cutting out of defects on the side sealing element (d)



**Figure 2.** Characteristics of the required cross-section of the deposited bead at restoration of HPT SNB side sealing element from ZhS6K alloy (a) and appearance of its surface restored by multilayer MPPS after liquid-penetrant testing (b, c)

that operational damage of nozzles from HTNA of ZhS32 type was repaired using practically the technologies of microplasma powder surfacing (MPPS) and laser-plasma surfacing with  $v_d$  of up to  $2 \text{ cm}^3$ , for instance, [2–5].

A priority task at development of the technology for restoration of the side sealing element of the above HPT SNB was evaluation of cracking susceptibility for a typical structure of ZhS6K alloy deposited by MPPS method (Figure 3) at successive increase of its volume in the direction of the respective increase of height  $H$  and length  $L$  of the deposited bead, in order to ensure the technological strength of such a welded joint (see Figure 2, b) in as-deposited condition.

**Table 2.** Results of static tensile testing of ZhS6K deposited metal in as-deposited condition (without heat-treatment)

Number, type	$T_{\text{test}}, ^\circ\text{C}$	$\sigma_{0.2}, \text{MPa}$	$\sigma_r, \text{MPa}$	$\varepsilon, \%$
1	20	1004	1004	0.5
2	900	639	641	0.8
3	1000	377	386.5	0.65
4	1100	–	256	0.1

Similar to previous work [6], devoted to assessment of cracking susceptibility of ZhS32 alloy at MPPS, respective evaluations in terms of determination of the main indices of total heat input into the product were conducted also for the deposited ZhS6K metal (Figure 4). It was established that no cracks form in the «base metal–deposited metal» welded joint of ZhS6 type alloy under the conditions of typical MPPS applications for restoration of blade shroud platforms ( $L \approx 35\text{--}40 \text{ mm}$ ;  $H \leq 5 \text{ mm}$ ;  $v_d \leq 2.0 \text{ cm}^3$ ). However, already at increase of bead length above  $L = 100 \text{ mm}$  during multilayer deposition of more than 5–7 mm height ( $v_d > 4\text{--}6 \text{ cm}^3$ ), the susceptibility to reheat cracking begins to be manifested in the deposited metal of ZhS6K alloy in most cases. Their appearance is due to the cumulative action of two factors: formation of residual longitudinal stresses [7] and established low deformability of the formed deposited ZhS6K metal (Table 2). Thus, the impossibility of ensuring the technological strength at application of ZhS6K alloy as deposited metal is established for the conditions of restoration of HPT SNB side sealing

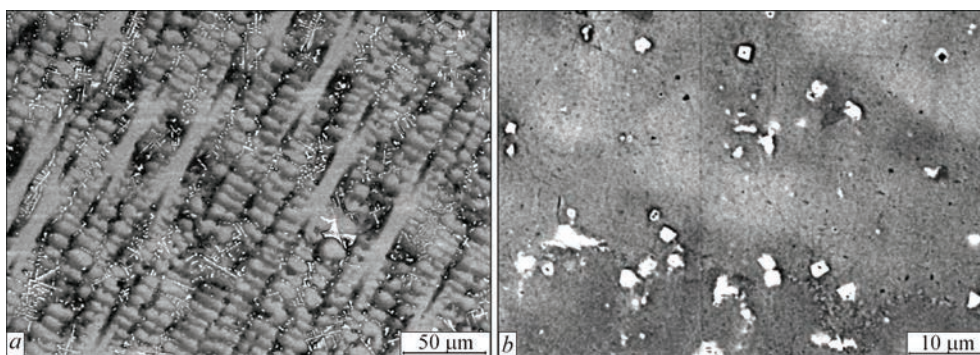


**Figure 3.** Microstructural features of ZhS6K deposited metal in as-deposited condition, scanning electron microscopy

element by multilayer MPPS, because of low deformability of the alloy during surfacing.

Periodical increase of deformability of ZhS6K deposited metal (to the level of  $\varepsilon_{1000\text{ }^\circ\text{C}} = 5.8\text{--}7.2\%$  [7]) by conducting vacuum heat treatment at the homogenization temperature could not be implemented in this HPT SNB, because of the design-technological limitations by the heat treatment temperature. They were due to the presence of brazed joints in it (sign hole cover, mounting threaded bushings), made using Vpr11-40N braze alloy. The temperature of such a brazed joint formation is much lower than that of ZhS6K alloy homogenization [8].

In view of impossibility of ensuring the technological strength at restoration of the side sealing element of HPT SNB at application of deposited metal of ZhS6K alloy, a decision was taken to apply deposited metal of reduced high-temperature strength. Static tensile testing of witness-samples of such deposited metal (Figure 5), conducted in servohydraulic machine MTS-810 by the procedure of [9], showed that the following level of short-term strength values is achieved compared to ZhS6K deposited metal: 0.7–0.8 at 20 °C and 0.5–0.55 at 1000 °C.

Compared to existing/known technology solutions that envisage application of filler materials of IN625 type with high-temperature strength  $\sigma_{t1000\text{ }^\circ\text{C}} \approx 110\text{ MPa}$ , the new technological approach, in addition to stable provision of technological strength of multilayer MPPS of volume  $v_d = 7\text{--}13\text{ cm}^3$ , allowed increasing the level of high-temperature strength of the deposited metal practically 2 times at 1000 °C and in addition effectively limited its high-temperature ductility  $\varepsilon_{1000\text{ }^\circ\text{C}} \leq 1.0\text{--}1.5\%$ . Considering the known level of service loads of this HPT SNB ( $\approx 20\text{ MPa}$  [1]), the assessed values of high-temperature strength of the deposited metal allow prediction of the presence of the required set of functional properties for its restored side sealing element, in particular spatial stability, necessary to ensure reliable operation in modern aircraft GTE of RD-33 type.

Proceeding from the materials of the conducted investigations, repair of a test batch of the above HPT SNB from ZhS6K alloy was conducted for Lutsk Repair Plant «Motor» by the technology developed at PWI (see Figure 2, c) and respective technological instructions were developed.

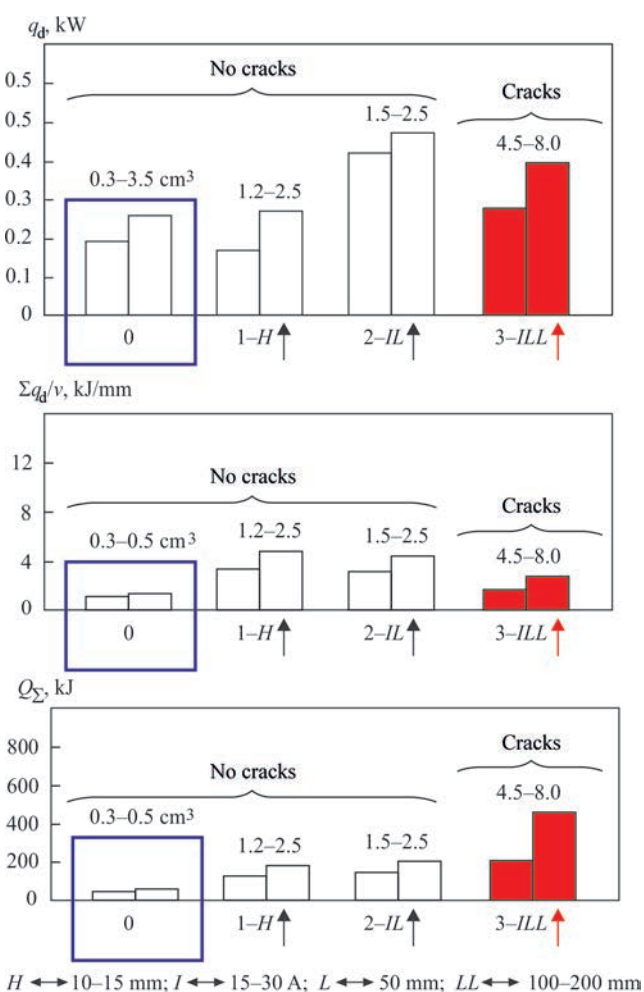


**Figure 4.** Analysis of the regularities of ensuring the technological strength in ZhS6K deposited metal, depending on a number of indices of the amount of heat input into the product ( $q_d$  — efficiency of microplasma arc;  $\Sigma q_d/v$  — sum of heat inputs of all the deposition layers;  $Q_\Sigma$  — total heat input into the product) and its volume. Technological variant «0» corresponds to the conditions of MPPS of shroud platforms of HPT blades, described in the text:  $H$  — 10–15 mm;  $I$  — 15–30 A;  $L$  — 50 mm;  $LL$  — 100–200 mm

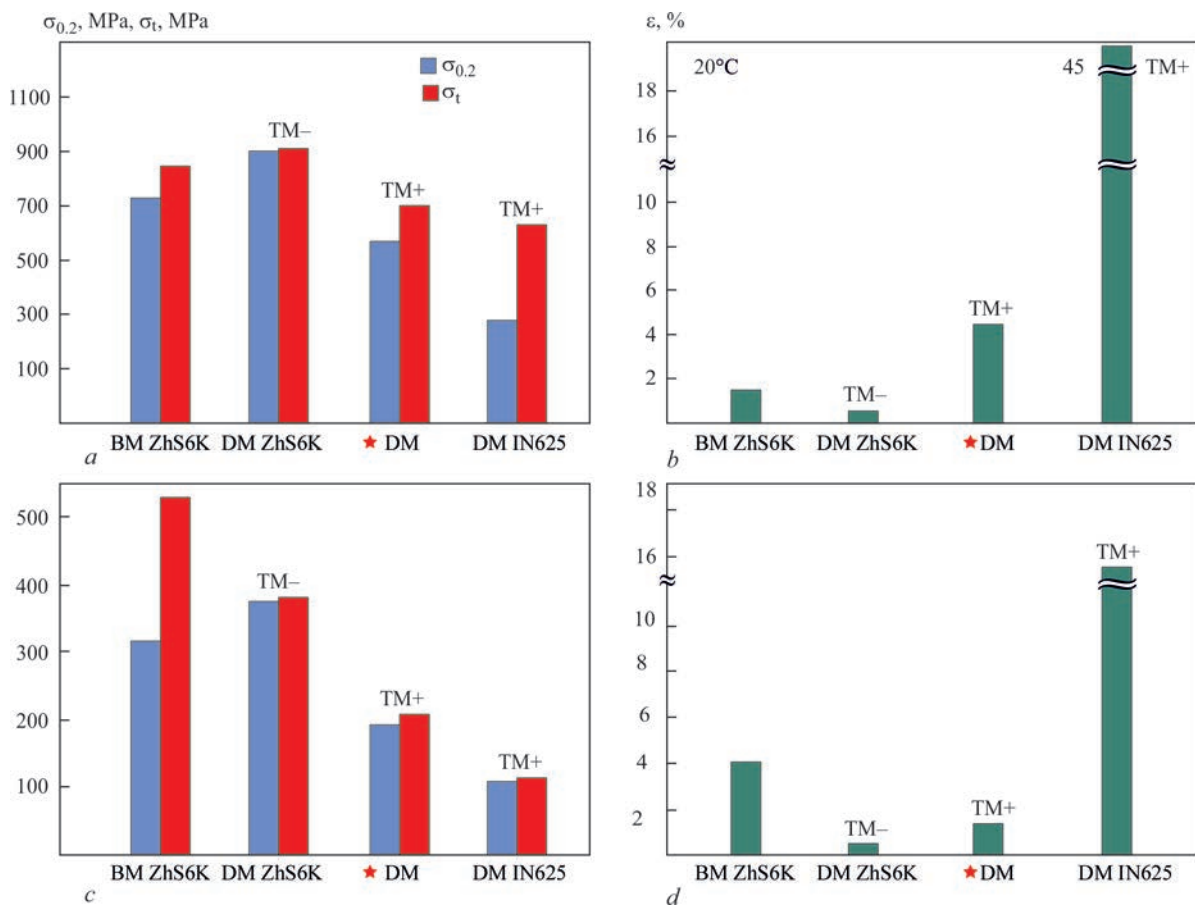


**Figure 5.** Analysis of short-time mechanical properties of different variants of deposited metal and regularities of ensuring its technological strength at restoration of HPT SNB side sealing element (BM — base metal; DM — deposited metal;  $\star$ DM — selected system of deposited metal; TS+ and TM- — technological strength is or is not achieved, respectively). Short-time mechanical properties of ZhS6K base metal are given by the data of [10]: a, b — 20; c, d — 1000 °C; (d —  $\times 25$ )

The work was performed under the integrated program of the NAS of Ukraine «Problems of residual life and safe operation of structures, constructions and machines in 2016–2020».

- Karpinos, B.S., Korovin, A.V., Lobunko, A.P., Vedishcheva, M.Yu. (2014) Operational damage of turboreactive bypass engines with afterburner. *Vestnik Dvigatelistroeniya*, **2**, 18–24 [in Russian].
- Yushchenko, K.A., Yarovitsyn, A.V. (2012) Improvement of technology for restoration of upper shroud of blades of aircraft GTE. In: *Problems of residual life and safe operation of structures, constructions and machines, NASU*. Kyiv, PWI, 506–509 [in Russian].
- Zhemanyuk, P.D., Petrik, I.A., Chigilejchik, S.L. (2015) Experience of introduction of the technology of reconditioning microplasma powder surfacing at repair of high-pressure turbine blades in batch production *The Paton Welding J.*, **8**, 39–42.
- Yushchenko, K.A., Yarovitsyn, A.V., Fomakin, A.A. et al. (2016) Development of technology of microplasma surfacing of ZhS32 alloy for reconditioning of gas-cooled blades of aircraft high-pressure turbine. In: *Problems of residual life and safe operation of structures, constructions and machines, NASU*. Kyiv, PWI, 696–701 [in Russian].
- Nerush, S.V., Ermolaev, A.S., Rogalev, A.M., Vasilenko, S.A. (2016) Investigation of the technology of restoration of blade airfoil edge of first stage high-pressure turbine from ZhS32-VI alloy by laser-powder surfacing method using the metal powder of ZhS32-VI alloy manufactured with atomization method. *Electron. J.: Trudy VIAM*, **44**(8), 24–34. DOI: <https://dx.doi.org/10.18577/2307-6046-2016-0-8-4-4>
- Yushchenko, K.A., Yarovitsyn, A.V., Chervyakov, N.O. (2017) Effect of energy parameters of microplasma powder surfacing modes on susceptibility of nickel alloy ZhS32 to crack formation. *The Paton Welding J.*, **2**, 2–6. DOI: <https://doi.org/10.15407/as2017.02.01>
- Yushchenko, K.A., Zvyagintseva, G.V., Yarovitsyn, A.V. et al. (2019) New approaches in evaluation of mechanical characteristics and microstructure of restored GTE parts from nickel high-temperature alloys. *Metalofizyka ta Novitni Tekhnologii*, **41**(10), 1345–1364 [in Ukrainian]. DOI: <https://doi.org/10.15407/mfint.41.10.1345>.
- Yermolaev, G.V., Kvasnytskyi, V.V., Kvasnytskyi, V.F. (2015) *Soldering of materials: Manual*. Ed. by V.F. Khorunov et al. Mykolaiv, NUK [in Ukrainian].
- Yushchenko, K.A., Yarovitsyn, A.V., Chervyakov, N.O. et al. (2019) Evaluation of short-term mechanical properties of a joint of difficult-to-weld nickel high-temperature alloys of ZhS6 type. *The Paton Welding J.*, **7**, 29–35. DOI: <https://doi.org/10.15407/as2019.07.07>.
- Kishkin, S.T. (2006) Development, investigation and application of high-temperature alloys. In: *Selected works*. Moscow, Nauka [in Russian].

Received 07.10.2020

## AUTOMATIC ARC SURFACING OF WORKING PATHS OF LIFT GATES OF KANIV NAVIGATION LOCK

**V.I. Galinich, V.M. Taganovskyi and G.V. Kuzmenko**

E.O. Paton Electric Welding Institute of the NAS of Ukraine

11 Kazymyr Malevych Str., 03150, Kyiv, Ukraine. E-mail: office@paton.kiev.ua

The paper gives the results of development and introduction of the technology of automatic arc surfacing of vertical embedded parts of navigation locks without dismantling them in the case of repair of rails of working paths of lift gates in the Kaniv navigation lock. 2 Ref., 8 Figures.

*Keywords:* navigation locks; lift gates, working path rails, automatic arc surfacing

Geographic position of Ukraine promotes development of its transportation potential, integration into the European transportation system, primarily as a country that takes a special place in providing transit cargo transportation with the most rational option for implementing West-East transport flows.

Four out of nine European transport corridors pass through the territory of Ukraine. The most important for inland water transport is corridor No.9 which connects the ports of White and Baltic Seas with those of Black Sea-Mediterranean basin.

Inland navigable river routes of Ukraine pass mainly through the waters of the Dnipro and Danube and, according to the European agreement on the major inland waterways of international importance they are classified as navigable river routes of the highest category E [1].

There are six shipping locks on the Dnieprovskiy cascade: Kyiv, Kaniv, Kremenchug, Dniprodzerzhynsk, ZRHS (Zaporizhzhya region of hydraulic structures) and Kakhovka.

A navigation lock is a hydraulic structure in the navigable and waterways to ensure the passage of vessels from one water basin (pool) to another with different water levels in them. It is limited on two sides by penstocks, located between which is the penstock chamber that allows controlling the water level within its limits. Transfer of ships with the help of a navigation lock is carried out by sequential passage to the penstock chamber after aligning the water level in them. Lock usage is mainly aimed at making navigable the water spaces with different water levels.

Each lock has three main elements:

- waterproof chamber, connecting the upper and lower parts of the channel and having a volume suffi-

cient for containing one or several vessels. Chamber position is fixed, but the water level in it may change;

- gates — metal shields, located at both ends of the chamber, which are used for letting the vessel into and out of the chamber before the beginning of locking and seal the chamber during locking.

- water supplying device, designed for filling or draining the chamber. A flat panel penstock is usually used as such a device. Transfer pumps can be used in large locks.

Kaniv shipping lock (Figure 1) is located at 727 river kilometre of the Dnipro river. The lock design was developed by Ukrainian Department of S.Ya. Zhuk Institute with the participation of SDB «Zaporizhhydroproekt», SDB «Lenhidroproekt» and «Ukrhidrorichtrans» Institute. The lock construction was carried out by the following trusts and associations: «Dniprobud», «Hidromontazh», «Hidrospetsbud», «Hidroelektromontazh», and «Spetshidroenergomontazh».

The lock was put into operation on 22.07.1972 by locking «T.G. Shevchenko» motor ship. The navigation chamber is 270 m long, 18 m wide, and design head is 12.75 m. Upper lock head is fitted with emergency flat gates and work lift gates. The lower head is fitted with work two-leaf gates, repair gates and penstocks. All the technological equipment of the lock



**Figure 1.** Kaniv navigation lock



Figure 2. Lift gates of Kaniv navigation lock



Figure 3. Support carriage of lift gates in Kaniv navigation lock work gates and penstocks is activated by volumetric hydraulic drives.

From the beginning of operation the lock performed 200470 lockings, with 477545 ships passing through it, i.e. the average monthly number of ships that have passed through the lock during the last year is equal to 97, while the design value is 34 (data as of 2017) [2].

In November, 2017 the Kaniv navigation lock was closed for internavigation repair to perform unique oper-

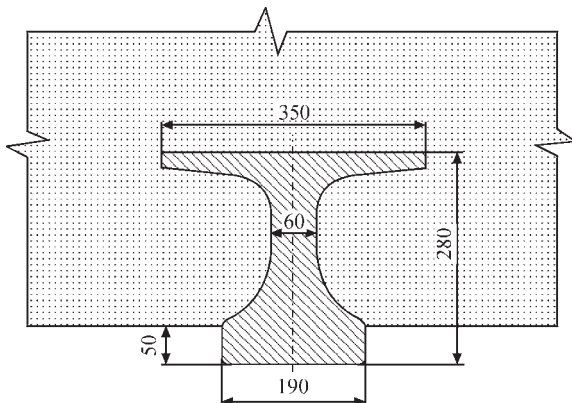


Figure 4. Cross-section of a concreted rail of the working path of lift gates in Kaniv navigation lock (schematic)



Figure 5. Characteristic damage of working path rails of lift gates in Kaniv navigation lock

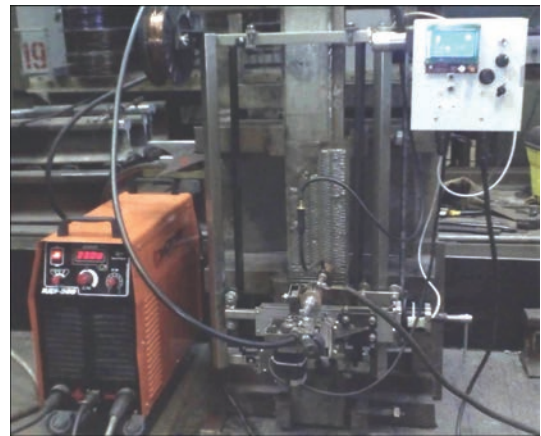
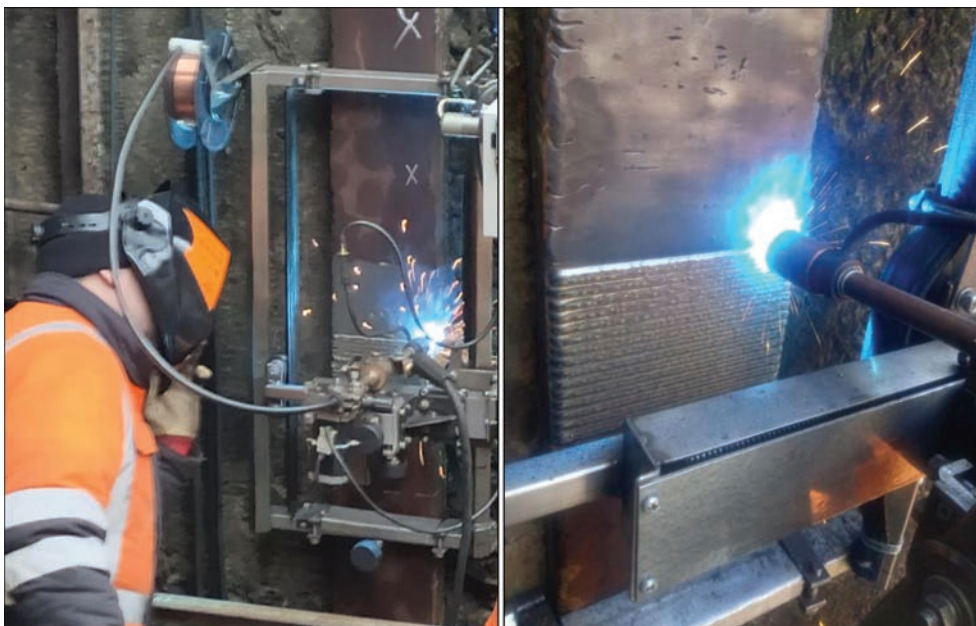


Figure 6. Specialized experimental equipment for automatic arc surfacing of vertical surfaces

ations on replacement of the work lift gates of the lock. The new gates were made by «Ukrhidromekh» Plant (Nova Kakhovka), and dismantling-mounting operations were to be performed by a specialized contractor «Kyivhidromontazh». It was planned to finish the work by May 2018, but because of a lack of funding it was moved to the internavigation period of 2019–2020.



Figure 7. Sample with a deposited region 150 mm wide and its cross-section



**Figure 8.** Automatic surfacing of working path rails of lift gates in Kaniv navigation lock

The work lift gates (Figure 2) take the water pressure and transfer it through the support carriage wheels to the embedded parts of the working paths (Figure 3), made in the form of cast rails from steel 45L to GOST 977, that were concreted during their installation in the walls of the guiding grooves of the lift gates (Figure 4). The load on the rails from each gate wheel is equal to 980 kN in the work zone.

Many years of operation resulted in accumulation on the rolling surface of the working path rails of damage in the form of a nonuniform mechanical wear and corrosion pits (Figure 5), the depth of which was equal to 3–5 mm. No cracks in the embedded element base metal or element deformations, not envisaged by design, were detected.

Under Project 8.8 «Development of the technology for repair and restoration of vertical guides of working paths of navigation lock lift gates in the water bodies of the Dniprovskiyi basin» of the Purpose-oriented Scientific Research Program «Problems of residual life and safe operation of structures, constructions and machines», PWI developed specialized experimental equipment (Figure 6) for automatic arc surfacing. It was used in the laboratory to optimize the technique and technology of gas-shielded surfacing ( $\text{CO}_2$ , Ar + + 21 %  $\text{CO}_2$  mixture) of vertical surfaces with 1 mm solid wire of Sv-08G2S grade. The above-mentioned equipment allows continuous surfacing of vertical regions of up to 220 mm size across the width and of up to 600 mm in the height, providing the deposited layer thickness within 2.5–4.0 mm in one pass (Figure 7).

Hardness of metal deposited on steel 45 sample is ensured in the range of *HB* 180 – 220, that is on the level of base metal hardness. This development was used at repair of the working paths of lift gates in the Kaniv navigation lock.

After measuring the working paths and their fault detection marking and scraping of the rail sections to be surfaced was performed. Scraping was conducted by electric grinders using steel brushes. The machine was fastened on the respective rail region and its surfacing was performed (Figure 8) across the entire width (190 mm) in the mode that guarantees the required geometrical parameters of the deposited layer. No preheating of the rail was applied, as self-heating of the base metal is ensured during continuous surfacing. After surfacing is over, the machine is moved to the next rail region.

Thus, on the whole, more than eleven linear meters of the right and left rails of the working paths were repaired, which were commissioned in June, 2020, after grinding and replacement of the gates.

The developed technology and equipment can further be used during repair performance in navigation locks and other facilities, where there is a need for surfacing the working surfaces of assemblies and parts of technological equipment without its dismantling, that will allow restoring their serviceability and extending their operating life.

1. Burmaka, I.O. (2014) Organization aspects of regulating navigation in internal waterways of Ukraine. *Mytna Sprava*, 1, 87–93 [in Ukrainian]. [http://nbuv.gov.ua/UJRN/Ms\\_2014\\_1\\_15](http://nbuv.gov.ua/UJRN/Ms_2014_1_15).
2. <http://ukrvodshliah.org.ua/index.php/kanivskyy-shluz/>

Received 13.10.2020

# DEVELOPMENT OF THE TECHNOLOGY OF SEMI-AUTOMATIC ARC WELDING FOR THE CONDITIONS OF OVERHAUL AND RECONSTRUCTION OF THE LINEAR PART OF THE MAIN GAS PIPELINES OF UKRAINE

**S.Yu. Maksymov, A.A. Gavrilyuk and D.M. Krazhanovskiy**

<sup>1</sup>E.O. Paton Electric Welding Institute of the NAS of Ukraine

11 Kazymyr Malevych Str., 03150, Kyiv, Ukraine. E-mail: [office@paton.kiev.ua](mailto:office@paton.kiev.ua)

More than 37 thou km of gas pipelines were laid through the territory of Ukraine. Their safe operation is based on proper technical maintenance and timely repair or reconstruction. At present manual arc welding is the main welding method used during performance of repair. Its low productivity necessitates shortening the duration of welding operations with simultaneous improvement of their quality. The objective of the work was development of the main principles and technology of semi-automatic arc welding of position circumferential butt joints of pipes of up to 1420 mm diameter inclusive that will enable shortening the time of welding operations performance, with the corresponding acceleration of laying of the restored sections of the main gas pipelines and simultaneous improvement of welded joint quality. Welding was performed by gas-shielded flux-cored wire OK Tubrod 15.19 of 1.2 mm diameter in Ar + CO<sub>2</sub> atmosphere and self-shielded flux-cored wire Coreshield 8 of 1.6 mm diameter. Analysis of the obtained results shows that the site of sample destruction is located in the base metal in all the cases. Such results indicate that the welded joint strength is higher than that of the base metal for these combinations of welding consumables and shielding gas. With the proper welding practices and strict adherence to the welding mode, butt joints of pipe steels comply with the normative documents, and flux-cored wire OK Tubrod 15.19 can be recommended for welding pipe steels of strength class K-60, while self-shielded flux-cored wire Coreshield 8 can be used for welding pipe steels of strength class K-52. 15 Ref., 6 Tables.

*Key words: main gas pipeline, semi-automatic arc welding, circumferential butt joint, flux-cored wire*

Pipeline network of Ukraine is characterized by considerable length (up to 37 thou km), large pipe diameters (up to 1420 mm inclusive), high working pressure (up to 7.4 MPa) and considerable service life (25 years and more). The latter circumstance makes stringent requirements of the linear part of the main gas pipelines in terms of ensuring the operational reliability and industrial safety [1, 2]. Safe operation of the main gas pipelines is based on proper engineering maintenance and timely repair or reconstruction [3, 4]. Repair performance envisages taking a package of technological measures, which are aimed at restoration of the main parameters and characteristics of the linear part of the main gas pipelines (LPMGP) up to design values [5–7].

Experience of repair operations in the main pipelines shows that manual arc welding is the most widely accepted method of their performance [8]. Practical experience shows that it takes a welders team of two workers not less than 5 h to weld just one circumferential position butt joint on a 1420 mm pipeline at wall thickness of 16 mm. That is why there is the need

for shortening the duration of welding operations with simultaneous improvement of their quality.

For economic conditions of Ukraine, solution of this problem is seen in the application of mechanized arc welding as a sufficiently simple and progressive method, on the one hand, and a comparatively inexpensive one, on the other. Application of solid wires allows increasing the productivity of welding operations by not less than 1.5–2.0 times, depending on the wire diameter. It is clear that increase of the diameter requires increase of the welding parameters for a stable running of the process of metal transfer into the weld pool. However, in welding in the modes, ensuring short-circuiting transfer of liquid metal into the pool, welding consumable consumption rises 1.5–3.0 times, as a result of spattering of liquid metal drops [9]. This results in greater time consumption, because of the need for additional cleaning of the welding zone from spatter [10]. Therefore, in order to keep a balance between welding productivity and welded joint quality, application of solid wires of up to 1.2 mm is acceptable in mechanized gas-shielded welding [11].

S.Yu. Maksymov — <https://orcid.org/0000-0002-5788-0753>, A.A. Gavrilyuk — <https://orcid.org/0000-0001-5443-6553>  
D.M. Krazhanovskiy Д.М. — <https://orcid.org/0000-0001-7292-7188>

© S.Yu. Maksymov, A.A. Gavrilyuk and D.M. Krazhanovskiy, 2020

**Table 1.** Modes of mechanized welding in different positions

Layer	Welding consumable	$V_w$ , m/min	$I_w$ , A	$U$ , V
Downhand position, 1G				
Root	Sv-08G2S	4.0	135	19.2
Filling	OK 15.19	9.4	207	28.4
	Coreshield 8	2.5	188	21
Facing	OK 15.19	9.4	210	28.2
	Coreshield 8	2.5	191	22
Vertical position, 3G				
Root	Sv-08G2S	2.8	103	18.8
Filling	OK 15.19	7.5	192	22.6
	Coreshield 8	2.5	202	23
Facing	OK 15.19	7.5	198	22.4
	Coreshield 8	2.5	214	24.2
Overhead position, 4G				
Root	Sv-08G2S	2.9	115	16
Filling	OK 15.19	8.0	185	26.3
	Coreshield 8	2.3	200	23.5
Facing	OK 15.19	7.5	180	26.0
	Coreshield 8	2.3	210	23

Rutile-type flux-cored wires for mechanized gas-shielded welding have quite significant advantages over solid wires, due to reduction of spattering and time required for scraping the deposited metal, 30–50 % increase of welding process productivity, ability to increase weld ductility by special alloying of the material [12]. The main advantage of self-shielded wires is believed to be the need for shielding gas application during welding. This feature enhances the mobility, facilitates operation performance under the field conditions, and eliminates the need for application of tents for protection from the wind. Unfortunately, the enterprises of SC «Ukrtransgas» now do not have any experience of application of these modern welding consumables.

The objective of the work as a whole was development of the main principles and technology of semi-automatic arc welding of circumferential position butt joints of up to 1420 mm pipes inclusive, that will enable reducing the time of welding operation performance with the respective acceleration of laying of the restored sections of the main gas pipelines with simultaneous improvement of welded joint quality.

In order to study the mechanical properties and impact toughness of butt welds, samples were welded in different positions with edge beveling by 30° to each side. Welding was performed using Evomig 500

**Table 2.** Chemical composition of materials, wt. %

Material	C	Si	Mn	Cr	Ni	Nb	Ti	Al	Mo	V	Cu	S	P
Sv-08G2S	0.09	0.065	1.65	–	–	–	–	–	–	–	–	–	–
OK 15.19	0.05	0.4	1.3	–	1.0	–	–	–	–	–	–	–	–
Coreshield 8	0.19	0.14	0.5	0.1	0.25	0.01	–	0.43	0.03	0.02	0.1	0.02	0.02
X70	0.08	0.26	1.60	0.03	0.03	0.062	0.002	–	–	–	–	0.006	0.022
09G2S	0.09	0.63	1.51	0.06	–	–	–	–	–	–	–	0.035	–

**Table 3.** Tensile testing of Mi-18 samples

Welding consumable	Position	Strength limit $\sigma_t$ , MPa	Sample destruction site
OK 15.19	Downhand, 1G	575.3	Base metal
Coreshield 8		504.1	Same
OK 15.19	Vertical 3G	579.1	»
Coreshield 8		505.2	»
OK 15.19	Overhead, 4G	570.9	»
Coreshield 8		503.3	»

semi-automatic machine in the downhand position with gas-shielded flux-cored wire OK Tubrod 15.19 of 1.2 mm diameter in Ar + CO<sub>2</sub> atmosphere and with self-shielded wire Coreshield 8 of 1.6 mm diameter. In both the cases, Sv08G2S wire of 1.2 mm diameter was used for root layer welding with Ar + CO<sub>2</sub> shielding.

In the first case, X70 steel plates of thickness  $t = 16$  mm were used as the base metal. Welding was performed in four layers: root, two filling and facing layer. In the second case, 09G2S steel 12 mm thick was selected as the material for welding. Welding was performed in five layers: root, three filling and facing layer. All the layers were made in one pass with transverse oscillations of the electrode (except for the root layer). Welding modes and chemical composition of the materials are given in Tables 1 and 2.

After welding, Mi-18 samples were cut out across the weld, which were tested by static tension. Test results are given in Table 3.

Analysis of the obtained results shows that the site of sample fracture is located in the base metal in all the cases. Such results indicate that the welded joint strength is higher than that of the base metal for these combinations of welding consumables and shielding gas. Therefore, further laboratory studies were aimed at determination of mechanical characteristics and impact toughness of the weld metal. During the experiment, performance of each subsequent pass was started at the moment, when the base metal temperature was 120–150 °C in the specified points at cooling. Results of weld metal testing are given in Tables 4 and 5.

Comparison of the obtained test results shows that the yield and strength limits of the metal of welds, made by gas-shielded wire OK 15.19 in different positions, are on the level of normative values of the base metal of pipes of K60 strength class. Ductility characteristic ( $\delta_5$ ) of the base metal is also higher than

**Table 4.** Mechanical characteristics of weld metal

Welding consumable	$\sigma_y$ , MPa	$\sigma_t$ , MPa	$\delta_5$ , %	$\psi$ , %
Downhand position, 1G				
OK 15.19	<u>467–491</u> 479	<u>598–603</u> 600.5	28.0	73.0
Coreshield 8	<u>382.2–374</u> 378.1	<u>532.1–533</u> 532.0	27.0	70.0
Vertical position, 3G				
OK 15.19	<u>567–571</u> 569	<u>669–679</u> 674	24.0	69.0
Coreshield 8	<u>327.8–389.7</u> 358.7	<u>503.0–518.5</u> 510.7	31.0	69.8
Overhead position, 4G				
OK 15.19	<u>534–541</u> 537.5	<u>648–653</u> 650.5	25.0	68.0
Coreshield 8	<u>354.0–384.0</u> 369	<u>514.0–517.0</u> 515.5	26.4	70.4

**Table 5.** Impact toughness (KCV) of weld metal

Welding consumable	Impact toughness $a$ , J/cm <sup>2</sup> at temperature, °C		
	+20	–20	–40
Downhand position, 1G			
OK 15.19	<u>137–173</u> 164	<u>126–160</u> 139	<u>98–101</u> 98
Coreshield 8	<u>122.3–151.5</u> 137.3	<u>70.2–135</u> 124.6	<u>64.2–84.3</u> 73.5
Vertical position, 3G			
OK 15.19	<u>109–154</u> 134	<u>99–111</u> 104	<u>82–99</u> 88
Coreshield 8	<u>127–152</u> 139	<u>90.3–115</u> 99.6	<u>54.2–58.4</u> 56.1
Overhead position, 4G			
OK 15.19	<u>109–152</u> 136	<u>116–143</u> 132	<u>67–99</u> 79
Coreshield 8	<u>124–143</u> 134.3	<u>87.1–89.2</u> 87.4	<u>48.4–52.0</u> 50.6

the minimum required one —  $\delta_5 \geq 24$  %. One can see that the values of mechanical characteristics are practically the same in welding in the downhand, vertical and overhead positions. At application of self-shielded wire Coreshield 8 the yield and strength limits of the weld metal are on the level of the normative values of the base metal of pipes of K50–K52 strength class. Ductility is higher than the minimum required one —  $\delta_5 \geq 20$  %. Impact toughness results are high even at testing temperature of  $-40$  °C of the Charpy samples.

In order to evaluate the limit ductility of the weld metal, testing of standard samples for static bending was performed. These tests allow assessment of the ability of the welded joints to withstand the specified plastic deformation, the magnitude of which is determined by the bend angle. For circumferential butt joints of pipelines, this angle should be less than  $120^\circ$ . In all the variants of the combinations of the

**Table 6.** Nitrogen [N] and oxygen [O] content in the deposited metal, %

Welding consumable	[N], %	[O], %
OK 15.19	0.0079	0.0428
Coreshield 8	0.0433	0.063

positions of welds and electrode wires, the bend angle was equal to  $180^\circ$ .

Analysis of the obtained results shows that with the proper welding practices and selected welding modes, the butt joints meet the normative requirements.

It is known that in gas-shielded welding of low-carbon and low-alloyed steels, such accompanying elements as nitrogen and oxygen are impurities [13, 14]. Under certain conditions, they can influence the lowering of welded joint ductility. Therefore, investigations were conducted with determination of the impact of shielding gases on the content of these elements in the weld metal. Investigation results are given in Table 6.

Obtained data show that a higher nitrogen content is recorded in welding with self-shielded wire Coreshield 8. There may be several reasons for this, namely higher voltage; poor gas shielding of the deposited metal from air. In self-shielded wires of carbonate-fluorite type, the gas shielding of the metal occurs due to carbonate decomposition. The quantity of nitrogen in the weld metal depends on the welding mode. It rises with increase of arc voltage. With greater length of the arc gap during the wire melting, the evolving gas can be insufficient to press the air away from the molten metal surface, partial pressure of nitrogen in the arc zone increases and its quantity in the metal becomes greater [15]. Increase of welding current will intensify the carbonate decomposition, but at the same time it will increase the nitrogen content in the deposited metal [11]. A more detailed answer can be given at thorough and directed performance of further experiments.

## Conclusions

1. Conducted investigations showed that the welded joints produced on X70 steel with application of gas-shielded wire OK Tubrod 15.19 in Ar + CO<sub>2</sub> mixture ensure mechanical characteristics of welded joint strength on the level of  $\sigma_t = 574$ – $580$  MPa, while mechanical characteristics of the weld metal in different positions are  $\sigma_t = 600$ – $670$  MPa.

Charpy impact toughness of weld metal is equal to  $79$ – $98$  J/cm<sup>2</sup> for  $-40$  °C temperature. Ductile characteristics of the weld metal are  $\delta_5 = 28\%$  that is higher than those specified for X70 steel ( $\delta_5 \geq 23$  %). Thus, summing up the resultant technological indices, as well as the obtained mechanical properties in welding X70 steel with gas-shielded wire OK Tubrod 15.19

in Ar + CO<sub>2</sub> mixture we can say that welding of pipe steels of strength class K-60 ( $\sigma_t = 588$  MPa) is permissible.

2. Obtained results of testing samples welded with self-shielded wire Coreshield 8 shows that strength ( $\sigma_t = 515$  MPa) and yield ( $\sigma_y = 369$  MPa) of the weld metal are on the level of normative values for base metal of pipes from steels of K-50–K-52 strength class. Charpy impact toughness of weld metal at testing temperature of  $-40^\circ$  is equal to 56–73 J/cm<sup>2</sup>.

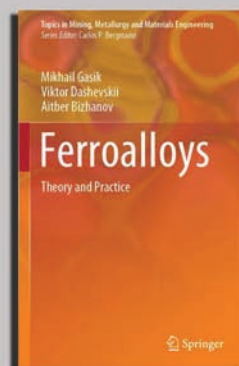
3. Analysis of the obtained results shows that with proper welding practices and strict adherence to the welding mode butt joints of pipe steels correspond to the normative documents.

*The work was performed under the integrated program of the NAS of Ukraine «Problems of residual life and safe operation of structures, constructions and machines in 2016–2020».*

1. Khrutba, V.O., Vaigang, G.O., Stegnii, O.M. (2017) Analysis of environmental hazards during operation and repair of main pipelines. *Ekologichna Bezpeka*, 24(2), 75–82 [in Ukrainian].
2. Poberezhnyi, L.Ya., Yavorskyi, A.V., Tsykh, V.S. et al. (2017) Increase of level of environmental safety of pipeline systems of gas-and-oil complex of Ukraine. *Tehnohenno-Ekologichna Bezpeka*, 1, 24–31 [in Ukrainian].
3. Fedorovych, I.V. (2013) Reliable operation of linear part of main gas-and-oil pipelines and examination of accident causes. *Agrosvit*, 5, 42–44 [in Ukrainian].
4. Bunko, T.V., Safonov, V.V., Strezhekurov, E.Ie., Matsuk, Z.M. (2018) Safety of long-distance gas transmission. *Geotekhnichna Mehanika*, 139, 106–115 [in Ukrainian].
5. Askarov, R.M., Tagirov, M.B., Kukushkin, A.N., Askarov, R.G. (2020) Repair of main pipelines. *Neftegaz RU*, 4, 140–145 [in Russian].
6. Shlapak, L.S., Prysyzhnyuk, P.M., Lutsak, L.D., Lutsak, D.L. (2017) Repair of corrosion-mechanical defects of main pipelines by method of flux-cored electrode surfacing. *Visti Donetskogo Girnychogo Instytutu*, 1, 254–257 [in Ukrainian].
7. Islamov, I.M., Chuchkalov, M.V., Askarov, R.M. (2018) Estimation of residual life of main gas pipeline under conditions of transverse corrosion stress cracking. *Transport i Khranenie Nefteproduktov i Uglevodородnogo Syria*, 2, 35–38 [in Russian].
8. Gorshkova, O.O. (2020) Welding of main gas-and-oil pipelines. *Sovremennye Naukoyomkie Tekhnologii*, 2, 7–11 [in Russian].
9. Lobanova, M.A., Klimovich, V.S., Fesenko, N.V. et al. (2019) Investigation of process productivity in consumable electrode gas-shielded arc welding (CO<sub>2</sub> and its mixture with argon) of low-carbon and low-alloy steels. In: *Proc. of 20<sup>th</sup> Republ. Student Sci.-Tekhn. Conf. on New Materials and Technologies of their Treatment. (Minsk, 17–18 April 2019)*, Minsk, BNTU, 90–92 [in Russian].
10. Potapievsky, A.G. (2007) *Consumable electrode gas-shielded welding*. Pt 1: Active gas-shielded welding. Kiev, Ekotekhnologiya [in Russian].
11. (1989) *Construction of main and industrial pipelines. Welding: DBN 006–89*. Introd. 1989-07-01. Minneftegazstroj SSSR [in Russian].
12. (1994) General specifications: GOST 26271–84. Flux-cored wire for arc welding of carbon and low-alloy steels. Introd. 1987-01–01. Moscow, Gosstandart SSSR [in Russian].
13. Pidgaetsky, V.V. (1970) *Pores, inclusions and cracks in welds*. Kyiv, Tekhnika [in Ukrainian].
14. Grigorenko, G.M., Lakomsky, V.I. (1968) Macrokinetics of nitrogen absorption by electrode metal from arc atmosphere. *Avtomatisch. Svarka*, 1, 10–14 [in Russian].
15. Suptel, A.M. (1976) *Mechanized flux-cored wire*. Kiev, Naukova Dumka [in Russian].

Received 28.09.2020

## NEW BOOK



Springer Publishing house (Switzerland) has released in 2020 a new book «Ferroalloys: theory and practice» (530 p.) by Gasik M.I., Dashevskii V.Ya., Bizhanov A.M., under supervision of Academician of National Academy of Sciences of Ukraine, Professor Mikhail Ivanovich Gasik.

This book outlines the physical and chemical foundations of high-temperature processes for producing ferroalloys with carbo-, silico- and aluminothermal methods, as well as technology practice for manufacturing of ferroalloys with silicon, manganese, chromium, molybdenum, vanadium, titanium, alkaline earth and rare earth metals, niobium, zirconium, aluminum, boron, nickel, cobalt, phosphorus, selenium and tellurium and also iron-carbon alloys. The chapters introduce the industrial production technologies of these groups of ferroalloys, the characteristics of charge materials, and the technological parameters of the melting processes. Special chapters are devoted to description of ferroalloy furnaces and self-baking electrodes in detail. Additionally, topics related to waste treatment, recycling, and solution of environmental issues are considered.

The book is recommended for specialists and researchers involved in the international ferroalloys production.

[www.springer.com/gp/book/9783030575014](http://www.springer.com/gp/book/9783030575014)

## DIAGNOSTICS OF HYDROGEN-OXYGEN PLASMA JET FOR APPLICATION IN THERMAL SPRAYING

Yu.S. Popil<sup>1</sup>, V.M. Korzh<sup>1</sup>, V.Ya. Chernyak<sup>2</sup> and Ye.A. Zakharov<sup>1</sup>

<sup>1</sup>NTUU «Igor Sikorsky Kyiv Polytechnic Institute»

37 Peremohy Prosp., Kyiv, Ukraine, E-mail: Popil\_kpi@ukr.net

<sup>2</sup>Taras Shevchenko National University of Kyiv

4g Akademik Glushkov Prosp., 03187, Kyiv, Ukraine

The problem of obtaining a low-temperature plasma jet, where the plasma-forming gas is a hydrogen-oxygen mixture produced by electrolysis-water generators, was considered. The aim of the work is to determine the size of the active zone of the jet, along the length of which the melting and heating of the particle takes place, and to control it by changing the nature of the flow. In the course of diagnosing the plasma jet, the distribution of temperature, velocity and effective thermal power depending on the nature of the jet flow was determined. It was determined that the sizes of the active zone of the plasma jet can be 1.4 times larger at a laminar nature of the flow than at a turbulent one. The maximum temperature is observed in the arc part of the plasmatron and amounts to  $8400 \pm 1000$  K, in the jet of hydrogen-oxygen plasma the average temperature is  $5000 \pm 500$  K. Taking into account the results of the diagnostics, the material for plasma spraying and distance can be chosen. 19 Ref., 1 Table, 2 Figures.

*Key words:* hydrogen-oxygen plasma jet, laminar, turbulent nature of flow, sizes of active zone of the jet, plasma spraying

The use of high-enthalpy gases and mixtures as a plasma-forming medium in the technologies of thermal coating is one of the modern research directions. It is known that to produce coatings with a high-quality performance applying thermal methods of deposition, the preference is given to the jets with high kinetic and thermal parameters, because an increase in these parameters leads to a more intense heat exchange between the plasma jet and sprayed particles.

The ability to control the power and specific energy characteristics of the plasmatron by changing the composition of the plasma-forming gas allows predicting the characteristics and comparative sizes of plasma jets obtained from different plasma-forming media. As a determining factor of efficiency of applying such a jet, the sizes of an active zone of a plasma jet can be chosen, in which heating, melting and acceleration of particles of the material during thermal spraying is possible.

Such a source can be a plasma jet using a hydrogen-oxygen mixture (HOM) as a plasma-forming medium, which is produced by electrolysis-water generators. Obtaining plasma-forming gas directly at the workplace makes the technological process of thermal treatment of materials mobile and the absence of cylinder, transport and storage facilities reduces the cost. In addition, in terms of influence on environment and human health, such a mixture during flaring

and plasma generation reduces the amount of harmful substances.

One of the components of the hydrogen-oxygen mixture is hydrogen, which during ionization has high thermophysical properties and is a highly efficient converter of electric energy into heat.

Analysis of the technical literature showed that the use of hydrogen-oxygen plasma in the processes of thermal treatment of materials is almost absent, and the use of hydrogen as a plasma-forming additive in the amount from 10 to 30 % in plasma-forming gases is an outdated information, more modern is the use of steam-water plasma [1–4].

Dissociation of hydrogen starts at a temperature of 2000 K, 90 % occurs at a temperature of 4700 K and ends completely at a temperature of 6000 K. In this temperature range, hydrogen has an extremely high thermal conductivity [5].

The temperature and enthalpy of hydrogen plasma under standard conditions are presented in Table. Depending on changes in physical conditions, these indices can increase significantly. During electric arc heating, the hydrogen-oxygen mixture as a plasma-forming gas can decompose into 23 neutral and charged components [6]. To simplify the determination of thermophysical properties, such dissociated products can be used as  $H_2$ , H,  $O_2$ , O, OH,  $H_2O + H$ . By theory, the dependence of enthalpy on plasma temperature of different gases can be determined using the reference literature [7, 8]. In practice, these physical characteristics and other may differ significantly,

taking into account changes in pressure, consumption and composition of the gas mixture.

The use of diatomic gases leads to a sharper increase in arc voltage (Table). In this case, the energy of the arc is also used to dissociate gas molecules into atoms. The arc voltage increases significantly while using a gas that has a high heat capacity and thermal conductivity.

The peculiarity of HOM is featured by the ratio between the volume of oxygen  $VO_2$  and hydrogen  $VH_2$  in the mixture obtained by electrolytic decomposition of water  $2H_2O = 2H_2 + O_2$ , constant and equilibrium  $\beta = VO_2/VH_2 = 0.5$ . At this ratio of components in the mixture, the plasma jet has an oxidizing potential.

A positive factor may be the fact that the presence of oxygen in hydrogen volume in the ratio 2:1 increases kinetic characteristics of the jet by increasing the density of the plasma-forming mixture.

However, oxygen as a plasma-forming gas has a lower ionization potential than nitrogen, so due to the lack of electrons, the oxygen atom will seek to compensate for it by electrons couple bound with hydrogen. As a result, HOM may have a lower ionization potential and a higher degree of dissociation than hydrogen, respectively, and the values of arc voltage will be lower than the values given in Table.

The choice of the mixture as a plasma-forming gas medium is determined by the possibility of its use in the existing plasmatron and a reliable operation of the anode and cathode units of this plasmatron, as well as the process technology.

The efficiency of using depends on the design of the plasmatron that generates plasma from the plasma-forming mixture. The main directions of improvement of typical designs of plasmatrons are oriented on modification of their separate units and elements to increase their efficiency factor [11].

Due to the fact that HOM is explosive, high safety requirements should be provided in the development of equipment and technological processes. Lack of information and investigations on the thermophysical characteristics of low-temperature hydrogen-oxygen plasma and evaluation of their impact on thermal processes hinders the development and implementation of HOM in the production.

The aim of the work was to generate low-temperature hydrogen-oxygen plasma of atmospheric pressure obtained by electric arc heating and to diagnose the thermophysical properties of the jet in relation to application in the plasma coating method.

For this purpose the following equipment was used: electrolysis-water generator of monopolar type A1803UKhLCh with the maximum efficiency on HOM production — 1.6 m<sup>3</sup>/g; power source of invert-

Data on plasma formation in different gases [9, 10]

Gas	Energy supplied to the plasmatron, kW	Plasma temperature, °C	Plasma heat capacity, kcal/kg	Voltage on the arc, V	Energy utilization factor for gas heating, %
Ar	48	14000	4670	40	40
He	50	20000	51100	47	48
N <sub>2</sub>	60	7300	9950	65	60
H <sub>2</sub>	62	5093	76600	120	80

er type CUT-40 for plasma cutting with an open-circuit voltage of 300 V and the maximum current of 40 A [12]. As the basis for the design of the plasmatron the cathode unit of the microplasma torch OB-1160A was used in the system MPU-4 [13].

The thermochemical cathode represents a water-cooling copper electrode containing a hafnium insert. The geometry of the plasmatron nozzle had a narrowing shape, the initial diameter was 3 mm. A safe operation, initiation and production of hydrogen-oxygen plasma were carried out with the help of starting gas mixtures, such as air. The start and receiving the plasma jet took place in air mixture, into which HOM was introduced, gradually the air mixture overlapped and a hydrogen-oxygen jet was formed. When the work is finished, the actions occur in reverse order. At a stable operation of the plasmatron on HOM, the operating voltage was 100 V.

**Procedure of investigations and results.** The geometric sizes of the plasma jet were fixed. The transition limits from a laminar to a turbulent nature of the flow were determined by maximum and minimum lengths of the plasma jet with the control of the mixture consumption. At a laminar nature of the flow, the consumption of the gas mixture was 0.4 m<sup>3</sup>/g and at a turbulent one more than 0.6 m<sup>3</sup>/g at a pressure of 0.08–0.1 MPa. As investigations of the geometry of a hydrogen-oxygen plasma jet with a laminar nature of the flow have shown, when the jet flows into the surrounding atmosphere, it behaves like a hydrogen-oxygen flame, the opening angle of the jet is small and can be 2–5°, and the length is more than 200 mm (Figure 1, *b*). With an increase in flow rates of the mixture and the transition of the jet into a turbulent nature of the flow, the opening angle increases and the plasma flame is reduced to 70 mm. As is seen from Figure 1, *a* (through a red light filter), the structure of the plasma flame resembles a gas flame, where the core and the near-core zone are visible.

To determine the effective thermal power of plasma jets of different flow nature, an experimental installation with a water calorimeter was used. The amount of heat emitted by the plasma jet was re-

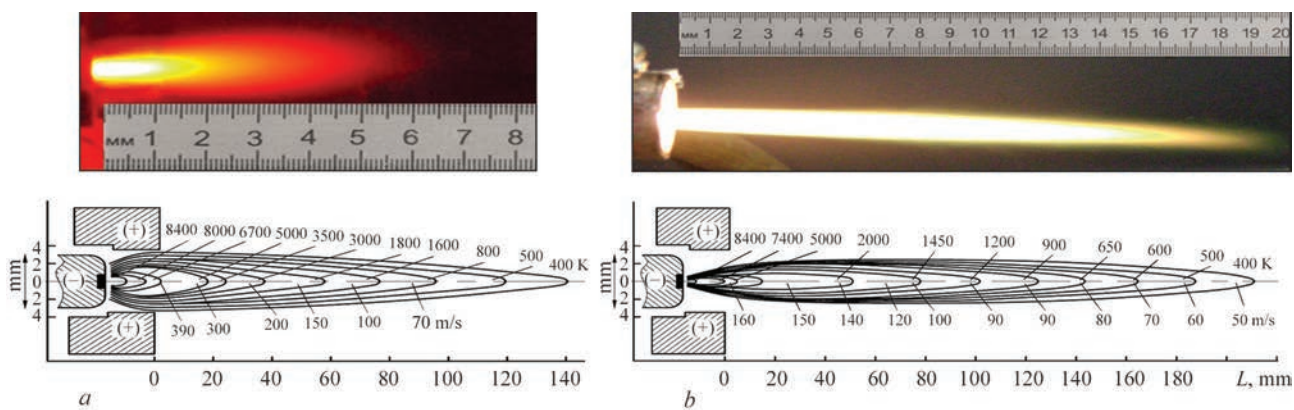


**Figure 1.** Distribution of temperature and velocity along the length of the plasma jet with different flow characteristics: *a* — turbulent  $V = 1 \text{ m}^3/\text{g}$ ; *b* — laminar  $V = 0.4 \text{ m}^3/\text{g}$

corded by heating the copper plate. At this time, the heating time, temperature of liquid in the calorimeter were determined, the measurement was performed by special Beckman thermometer, and calculations were performed according to the standard method [14].

The studies showed that the effective thermal power at a consumption of HOM being  $0.4 \text{ m}^3/\text{g}$ , which corresponds to a laminar nature of the flow, amounted to 30 mJ at an applied electric power to the plasma-tron of 4 kW. At perturbation of a flow and transition to a turbulent state of a flow with a consumption of the mixture being  $0.6\text{--}1.0 \text{ m}^3/\text{g}$ , the effective thermal power amounted to 54–60 mJ.

The hydrodynamic method was used to determine the velocity distribution along the jet length applying a probe based on a Pitot-Prandl tube with a diameter of 1.5 mm and inner holes of 0.5 mm. To calculate the velocity, an equation known from technical thermodynamics based on the Bernoulli equation was used, which takes into account the pressure and plasma temperature in the jet region [15].

To study the temperature distribution along the length of the plasma jet, the jet was divided into three intervals of effective temperatures. Three methods of measurement were used: in the temperature range of 8000–4000 K — spectral one, 3300–2200 K — pyrometric one and 2000–500 K — thermocouple one.

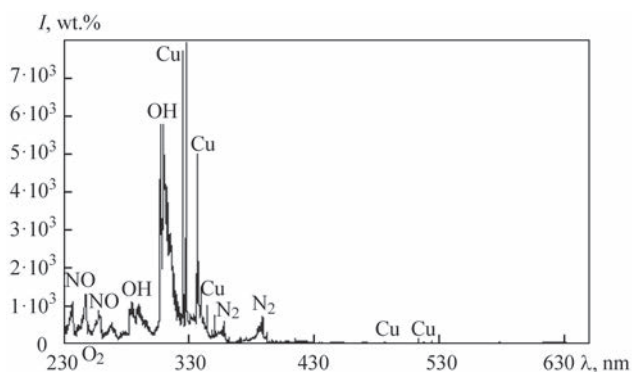


**Figure 2.** Spectra of plasma flame radiation at  $z = 15 \text{ mm}$ ,  $h = 5 \text{ mm}$  in the wavelength range of 200–650 nm

To determine the temperature in the first range based on the components of the plasma jet, the noncontact method of emission spectroscopy was used. To study the second temperature range, an optical pyrometer LOP-78 was used based on the temperature of the heated body, where as a body a tungsten rod with a diameter of 3 mm was used, the absolute temperature was calculated according to the standard procedure [16]. In the third range, a tungsten-rhenium thermocouple VR-5/20 with a diameter of 0.5 mm was used. To prevent oxidation and burnout, the thermocouple was placed in a protective shell of quartz glass. The thermocouple was calibrated, the error of thermocouples amounted to 1 % of the electromotive force measurement, and the admissible error of the measuring device was 0.2 %. To determine the temperature of the plasma jet components, the noncontact method of emission spectroscopy was used. The temperatures and concentrations of the components of the plasma jet were studied along its length ( $z$ ), at a deviation from the central axis ( $h$ ), taking into account the fact that the torch is axisymmetric.

The emission spectra of the plasma flame were recorded using a spectrometer based on the CCD line Solar TII (S-150-2-3648 USB), which operates in the wavelength range of 200–1080 nm and has a triangular hardware function with a half-width of 0.2 nm, in the wavelength range of 200–650 and 0.3 nm in the range of 650–1080 nm. The radiation was recorded on the rays of vision perpendicular to the axis of the plasma flame [17, 18]. Figure 2 shows typical spectra of plasma radiation in the case of using HOM at  $z = 15 \text{ mm}$  and  $h = 5 \text{ mm}$ . The spectra are multicomponent, containing components of the electrode material, namely, atomic copper lines, components of the atmosphere, into which the jet flows, and the working gas, oxygen multiplet and molecular bands OH, NO,  $\text{O}_2$  and  $\text{N}_2$ .

The values of the excitation population temperatures of the electronic  $T_e^*$  levels were determined using the software code Spec Air [19].

The calculations and experiments showed that the temperatures determined on copper are  $T_e^*$  (Cu) =  $6700 \pm 1000$  K. The temperature of atomic oxygen on the axis of the plasma flame is twice higher as compared to the random deviation from the axis, i.e. at  $h = 0$  mm  $T_e^*$  (O) =  $8400 \pm 1000$  K, and at  $h = 5$  mm  $T_e^*$  (O) =  $4100 \pm 1000$  K. The population temperature of the excited oscillatory and rotational levels of hydroxide within the error is the same and equals to  $T_r^*$  (OH) =  $T_v^*$  (OH) =  $5000 \pm 500$  K. The excitation population temperatures of the electron  $T_e^*$  oxygen levels, determined by the method of Boltz charts, have a lower value as compared to the use of the software code Spec Air, but these differences do not exceed the error value. The temperatures that were determined by the molecule (OH) and by the atomic components (O and Cu) differ, which indicates that the plasma is nonisothermal. The reason for the temperature difference may be a nonuniform spatial distribution of radiating particles and exothermic processes in the flame. As was shown by estimation of the population temperatures of the excited electronic levels along the length of the hydrogen-oxygen plasma jet, as the average mass temperature of the jet the value of the OH molecule, which represents  $5000 \pm 500$  K, can be taken, and as the maximum atomic mass O =  $8400 \pm 1000$  K, which coincide with the literature data.

A study in the temperature range of 3300–900 K showed that the distribution largely depends on the nature of the flow, and at a laminar nature of the flow (Figure 1, *b*), this area can be 1.4 times larger in relation to a turbulent one (Figure 1, *a*). At the turbulence of a flow the tendency changes, a more high-temperature interval 8000–4000 K is larger at a turbulent nature of a jet flow.

The maximum values of the plasma jet velocity grow in the case of increased flow rates at a constant nozzle diameter, which is characteristic of a turbulent nature of the flow, but as the flame length shortens, the range of effective velocities also decreases. With a decrease in the flow rates of the mixture and the transition to a laminar nature of the flow, the maximum values of the velocities are lower, but the length of the interval of effective velocities is larger.

Taking into account the effective temperature and velocity intervals of the plasma jet using HOM as a plasma-forming gas, it is possible to set the sizes of the active zone of the jet, in which melting and a sufficient velocity of particles are possible, to determine one of the important technological parameters of the process of thermal coating, spraying distance and to

produce a quality coating. This distance for such process parameters can be 80 mm for a turbulent and 140 mm for a laminar nature of the jet flow.

Accordingly, the velocity values of the jet can be significantly increased by increasing the flow rate of the plasma-forming mixture, initial diameters and profiling of geometric sizes of the nozzle part of plasmatoms. Meantime, the lengths of the plasma jet as well as the sizes of the active zone may change. However, the regularity of the temperature distribution in the jet of a hydrogen-oxygen plasma may correspond to the results of our investigations.

For application of the plasma method of spraying functional coatings using HOM as a plasma-forming gas, the following approach can be defined. At a laminar nature of the flow, it is possible to apply coatings from metals and alloys. At a turbulent nature it is more effective to spray heat-resistant, heat-protective and other coatings based on oxides, borides, etc., with a high melting point.

## Conclusions

1. The distance of spraying while using HOM can be 1.4 times larger during a laminar nature of the jet flow than during a turbulent one. The angle of opening of the jet is  $2\text{--}5^\circ$ , which allows concentrating the heat flux density on the treated product by reducing the heating spot.

2. The effective thermal power of the plasma jet at a flow rate of HOM being  $0.4\text{ m}^3/\text{g}$ , which corresponds to a laminar nature of the jet flow, was 30 mJ, at a supplied electric power to the plasmatron being 4 kW. At a turbulent nature of the plasma jet flow at a flow rate being  $0.6\text{--}1.0\text{ m}^3/\text{g}$ , the power was 54–60 mJ.

3. The maximum temperature of the hydrogen-oxygen plasma is observed in the arc part of the plasmatron and at the nozzle-anode section of 9–12 mm and amounts to  $8400 \pm 1000$  K, the average mass temperature of the hydrogen-oxygen plasma jet is  $5000 \pm 500$  K.

4. The presented results can be used in the development of technological processes of plasma method of coating using HOM as a plasma-forming gas.

1. Nikolaev, G.A., Olshansky, N.A. (1975) *Special methods of welding*. Moscow, Mashinostroenie [in Russian].
2. Borisov, Yu.S. (1987) *Thermal coatings from powder materials*: Refer. Book. Kiev, Naukova Dumka [in Russian].
3. Korzh, V.M., Popil, Yu.S. (2010) *Hydrogen-oxygen flame treatment of metals*. Kiev, Ekotekhnologiya [in Russian].
4. *By data of Companies LLC Multiplaz*. <http://www.multiplaz.ru/> OJSC Elion, Gorynych <https://as-pp.ru/gorynych>; <http://aspromt.ru/mppk-gorynych> [in Russian].
5. Frolov, V.V. (1954) *Physicochemical processes in welding arc*. Moscow, Mashgiz [in Russian].

6. Dudko, D.Ya., Emets, Yu.P., Repa, I.I. (1981) Composition and electrophysical parameters of hydrogen-oxygen plasma. *Teplofizika Vysokikh Temperatur*, 19(4), 697–701 [in Russian].
7. Dautov, G.Yu., Uryukov, B.A. et al. (2004) Generation of low-temperature plasma and plasma technologies. In: *Problems and Prospects*. Novosibirsk, Nauka, 105–145 [in Russian].
8. Vargaftik, N.B. (1963) *Reference book on thermophysical properties of gases and fluids*. Moscow, Fizmatgiz [in Russian].
9. (1959) Browning. Plasma — a substitute for the oxy-fuel flame. *Welding J.*, 9, 38.
10. Vasiliev, K.V., Isachenko, A.A. (1962) On application of plasma heating in welding processes. *Trudy VNIIVTOGEN*, Issue 8 [in Russian].
11. Zhukov, M.F., Smolyakov, V.Ya., Uryukov, B.A. (1973) *Electric arc heaters of gas (plasmotrons)*. Moscow, Nauka [in Russian].
12. Korzh, V.M., Popil, Yu.S., Popil, N.Yu., Moskalenko, D.B. (2015) *Method of producing of hydrogen-oxygen plasma jet*. Ukraine Pat. 107568, fill. 31.12.2015; publ. 10.06.2016; Int. Cl. H05H1/26, B23K 10/02, B23K 101/00 [in Ukrainian].
13. Paton, B.E., Gvozdetzky, V.S., Dudko, D.A. et al. (1979) *Microplasma welding*. Kiev, Naukova Dumka [in Russian].
14. Rykalin, N.N. (1985) *High-temperature technological processes*. Moscow, Nauka [in Russian].
15. Abramovich, G.N. (1969) *Applied gas dynamics*. Moscow, Fiz-Mat. Literatura [in Russian].
16. (1977) *Optical pyrometer LOP-72*: Certificate. Kharkov, Oblgrafizdat [in Russian].
17. Laux, C.O., Spence, T.G., Kruger, C.H., Zare, R.N. (2003) Optical diagnostics of atmospheric pressure air plasma. *Plasma Sources Sci. Technol.*, 12 (2), 125–138.
18. (1985) Electron-excited molecules in nonequilibrium plasma. *Trudy FIAN*. Moscow, Nauka [in Russian].
19. Pearse, R.W.B., Gaydon, A.G. (1976) *The identification of molecular spectra*. John Wiley & Sons, Inc., New York.

Received 12.10.2020

## SUBSCRIPTION



«The Paton Welding Journal» is Published Monthly Since 2000 in English, ISSN 0957-798X, doi.org/10.37434/tpwj.

«The Paton Welding Journal» is Cover-to-Cover Translation to English of «Automatic Welding» Journal Published Since 1948 in Russian and Ukrainian.

«The Paton Welding Journal» can be also subscribed worldwide from catalogues subscription agency EBSCO.

If You are interested in making subscription directly via Editorial Board, fill, please, the coupon and send application by Fax or E-mail.

12 issues per year, back issues available.

\$384, subscriptions for the printed (hard copy) version, air postage and packaging included.

\$312, subscriptions for the electronic version (sending issues of Journal in pdf format or providing access to IP addresses).

Institutions with current subscriptions on printed version can purchase online access to the electronic versions of any back issues that they have not subscribed to. Issues of the Journal (more than two years old) are available at a substantially reduced price.

The archives for 2009–2018 are free of charge on [www://patonpublishinghouse.com/eng/journals/tpwj](http://www://patonpublishinghouse.com/eng/journals/tpwj)

## ADVERTISING in «The Paton Welding Journal»

### External cover, fully-colored:

First page of cover  
(200×200 mm) — \$700  
Second page of cover  
(200×290 mm) — \$550  
Third page of cover  
(200×290 mm) — \$500  
Fourth page of cover  
(200×290 mm) — \$600

### Internal cover, fully-colored:

First/second/third/fourth page  
(200×290 mm) — \$400

### Internal insert:

(200×290 mm) — \$340  
(400×290 mm) — \$500

- Article in the form of advertising is 50 % of the cost of advertising area

- When the sum of advertising contracts exceeds \$1001, a flexible system of discounts is envisaged

- Size of Journal after cutting is 200×290 mm

### Address

11 Kazymyr Malevych Str. (former Bozhenko Str.), 03150, Kyiv, Ukraine

Tel.: (38044) 200 60 16, 200 82 77

Fax: (38044) 200 82 77

E-mail: [journal@paton.kiev.ua](mailto:journal@paton.kiev.ua)

[www://patonpublishinghouse.com/eng/journals/tpwj](http://www://patonpublishinghouse.com/eng/journals/tpwj)